https://doi.org/10.5194/nhess-2024-152
Preprint. Discussion started: 19 September 2024

Natural Hazards and Earth System Sciences
Discussions

Derivation of Moisture-Driven Landslide Thresholds for Northeastern Regions of the Indian Himalayas

Danish Monga[1], Poulomi Ganguli[1*]

[1]Agricultural and Food engineering department, Indian Institute of Technology Kharagpur, Kharagpur India

*Correspondence to: Poulomi Ganguli (pganguli@agfe.iitkgp.ac.in)

Abstract

Landslides pose a significant threat in the Northeastern Himalayas, driven by monsoonal rains and exacerbated by rapid urbanization. This research establishes moisture (primarily rainfall) thresholds that can cause landslides in Northeastern Himalayas 'hotspots' based on 490 rain-driven landslides catalogued between 2006 and 2019. Coupling the innovative Regularized Expectation-Maximization approach with non-crossing quantile regression, we reveal critical insights into antecedent moisture conditions and their role in shallow to deep landslide genesis. Our derived moisture threshold for the Northeastern Himalayan region, E (mm) = -11.10 + 0.62 D (hour), for 24 < D <1440 *hr*, fits within global bounds for both deep and shallow landslides. The spatial analysis demonstrates significant heterogeneity, with Guwahati (located at 26.14° N, 91.74° E in Assam) and Shillong (located at 25.58° N, 91.89° E in Meghalaya) requiring higher cumulative rainfall for landslide triggers compared to Aizwal (located at 23.73° N, 92.72° E in Mizoram). Our analysis shows that environmental controls, e.g., elevation, slope, land use types, CND, and rock types, play significant roles in shaping rainfall thresholds to trigger landslides. The insights from this research offer effective landslide risk management strategies and advance the predictive capabilities of Landslide Early Warning Systems with broader implications for climate resilience and disaster preparedness.

1 Introduction

Landslides, which accounted for to around 5% of all natural disasters globally between 1990 and 2005 (EM-DAT, 2023), severely threaten both lives and infrastructure, causing extensive economic and human

https://doi.org/10.5194/nhess-2024-152
Preprint. Discussion started: 19 September 2024


Natural Hazards and Earth System Sciences Discussions

losses each year. The Himalayas, particularly the Indian Himalayan region, are notably vulnerable, accounting for approximately 15% of the global landslides recorded between 2004 and 2017 (Das et al., 2023; Froude and Petley, 2018; Poornima et al., 2024; Sharma, 2021). Increased water infiltration from rain and snowmelt causes moisture-driven landslides (MDLs), which raise subsurface moisture levels, exacerbating the risk of landslides (Johnston et al., 2021; Monga and Ganguli, 2024; Whiteley et al., 2019). A recent report in May 2024 highlighted a surge in landslides in the NE region, attributing the increase to heavy monsoon rains and unplanned urban development, emphasizing an urgent need for robust mitigation efforts (Telegraph India, 2024). Rainfall, a crucial driver, not only increases the pore pressure but also decreases the effective stress of the soil, reducing soil shear strength and eventually making slopes more susceptible to failure(Lepore et al., 2013; Liu et al., 2024; Ravindran and Gratchev, 2021). The intensifying risk is further compounded by rapid urbanization, the expansion of infrastructure in landslide-prone areas, and altered precipitation dynamics due to climate change (Intergovernmental Panel On Climate Change (Ipcc), 2023). The variability in landslide triggers, ranging from low-intensity prolonged rains causing high degree of sub-surface percolation to high-intensity short-duration rain events linked to erosion and floods, underscores the complexity of predicting and managing these hazards (Tsunetaka, 2021; Zhang and Liu, 2010). NE Region of India (hereafter NERI; see Figure 1), which comprises eight Indian states, namely, Arunachal Pradesh, Assam, Manipur, Meghalaya, Mizoram, Nagaland, Sikkim, and Tripura, are susceptible to various degrees of landslides due to a combination of steep terrain of the northeast (NE) Himalayan range, extreme rainfall, earthquakes and other anthropogenic activities. According to the most recent report from 2023, most landslides over the NERI are shallow translational (planar) types triggered by rainfall, accounting for approximately 19% of landslides in India (Jain et al., 2023). Therefore, the implementation of an effective climate-informed Landslide Early Warning System (LEWS) in the Northeastern Himalayan (NEH) has become crucial. While such systems can facilitate timely evacuations and potentially save lives and are vital for advancing landslide prediction and mitigation(Harilal et al., 2019; Ramesh et al., 2023), an understanding of the intricate interactions between hydrometeorological conditions, terrain, and land surface processes across the NEH remains elusive owing to sparser observational networks, steep and inaccessible terrain, and heavy monsoon rainfall in much of this region.

https://doi.org/10.5194/nhess-2024-152
Preprint. Discussion started: 19 September 2024


Natural Hazards and Earth System Sciences Discussions

Empirical thresholds for rainfall-induced landslides are crucial in developing the LEWS, serving as essential tools for predicting and mitigating landslide hazards (Dixit et al., 2024; Jordanova et al., 2020; Singh and Kumar, 2021). Several studies have established rainfall thresholds across various regions of India; however, significant gaps remain, particularly in the NEH. For instance, Harilal et al. (2019) identified rainfall thresholds in Sikkim, while Mandal and Sarkar (2021) and Abraham et al. (2022) focused on the Darjeeling Himalayan region, demonstrating the effectiveness of empirical thresholds in landslide prediction. These studies, however, often overlook the unique geological and climatic conditions of the NEH (Abraham et al., 2022; Harilal et al., 2019; Mandal and Sarkar, 2021) and have considered at-site (gauge) rainfall time series with limited observations to derive rain thresholds. Recently, Saha and Bera (2024) investigated rainfall thresholds using five stations across western Himalaya, which utilize NASA POWER rainfall products. Although NASA POWER rainfall products are helpful for large-scale applications, they lack finer spatial resolution, being available at 0.5° x 0.625° latitude/longitude grids. Hence, their credibility in capturing extreme events and local scale variability is limited, leading to potential underestimations in regions with complex terrain (Setiya et al., 2024; NASA POWER, 2024). A significant limitation of the current state-of-the-art practices in the LEWS development is the lack of comprehensive regional studies addressing the finer spatial variability of MDL thresholds required for credible landslide predictions.

Second, while a few assessments in India and elsewhere in the Aisa have considered event-based rain events and assumed to follow a power-law relationship between rainfall intensity-duration (*ID*) (Choo et al., 2024; Das and Ganguli, 2022; Dikshit and Satyam, 2018; Kim et al., 2021; LIU et al., 2023), the total rainfall-duration (*ED*) space can consider two different storm types responsible for landslides (Leonarduzzi and Molnar, 2020): short-duration intense storm events and antecedent moisture content (AMC), resulting from long-duration persistent rain events with less intensity. The AMC significantly influences landslide initiation by pre-saturating the soil, reducing its strength, and making it more susceptible to slope failure during subsequent rainfall events(Bogaard and Greco, 2018). This motivates the importance of Event-Duration (ED) moisture thresholds, which consider both the duration of rainfall events and the antecedent moisture conditions, responsible for landslide triggers, thereby enhancing the predictability and effectiveness of the LEWS.

https://doi.org/10.5194/nhess-2024-152
Preprint. Discussion started: 19 September 2024


Natural Hazards and Earth System Sciences
Discussions

Third, very few studies have so far linked rainfall thresholds to trigger landslides with potential environmental controls, despite their critical role in landslide susceptibility. The influence of environmental controls, *e.g.*, Land Use/Land Cover (LULC) (Bourenane and Bouhadad, 2021), slope (Zhao et al., 2023), Topographic Wetness Index (TWI) (Sørensen et al., 2006), and Channel Network Distance (CND) (Godt and McKenna, 2008), is well established in the literature. The review of the literature (Singh et al., 2024; Yesuph and Dagnew, 2019) suggests that regions with dense forests and robust rock formations typically require higher rainfall to trigger landslides. This finding is further supported by an earlier assessment (Peruccacci et al., 2017), who demonstrated that forests and areas underlain by strong rock structures generally demand more rainfall to initiate landslides. Understanding the contributions of potential environmental controls in shaping spatial variability of rain thresholds is hence critical to inform landslide risk and enhancing the predictive capabilities of LEWS.

This study adds value to the existing state-of-the-art in moisture-driven landslide prediction by enhancing methodological practices in MDL threshold development on multiple fronts: (1) We reconstructed the gauge-based daily rainfall time series of the NERI using the Regularized Expectation-Maximization (RegEM) approach, a method extensively applied in climate studies (Li et al., 2005.; Schneider, 2001), to obtain a long-term continuous rainfall series. (2) Unlike earlier studies, which simply relied on graphical measures to determine lag-times for the AMC, we estimate the optimal lag-time of the AMC on landslide genesis by employing a quantitative approach considering (a) the scaling-relationship between accumulated versus triggering rainfall (Aleotti, 2004; Dikshit et al., 2019), considering the concept of "scattering bias" from the literature (Dahal and Hasegawa, 2008), and (b) the non-parametric dependence measure, Kendall's τ considering 3 to 60 days lag times. (3) we employed non-crossing quantile regression to derive moisture ED thresholds, ensuring monotonic and accurate quantile estimates that address the limitations of ordinary quantile regressions(Liu and Wu, 2009). Second, from an operational perspective, our study develops MDL thresholds considering a large array of landslide-prone sites across the NERI and derives a regional rain threshold curve to trigger MDLs, aiming to contribute effective LEWS. For this, we seek to understand the effects of triggering versus antecedent moisture contents on landslide genesis and assess landslide hazards by formulating regional and at-site ED rainfall threshold curves. Finally, we link the rainfall thresholds for triggering MDLs with potential

https://doi.org/10.5194/nhess-2024-152
Preprint. Discussion started: 19 September 2024


Natural Hazards and Earth System Sciences Discussions

environmental controls, establishing an association between physical drivers and the spatial variability in these rain thresholds across different sites, which is lacking for the NEH region.

Acknowledging the challenges posed by inconsistent rainfall records, spatial heterogeneity, and land use changes, we emphasize that our approach provides an effective LEWS framework by considering both antecedent and triggering rain events in developing ED thresholds that can aid in the operational forecast of climate-induced landslides (Guzzetti et al., 2020). The insights drawn from this research extend beyond the NEH to other regions with similar geophysical characteristics, aiding community resilience and mitigating landslide hazards.

2 Study Area and Data

The focus of this investigation is the NE regions of the Himalayas. Figure 1 shows the NERI area and the locations of eight hydrometric observatories that are situated within highly landslide-susceptible urban areas of the NEH range (Jaiswal, 2023). These eight hydrometric observatories are part of major glacial melt river basin systems, such as Mahananda (Darjeeling), Teesta (Kalimpong and Gangtok), Barak (Aizwal), Brahmaputra (Guwahati and Shillong), Dhansiri (Kohima), and Manipur River Basin (Imphal). Figure S1 shows the landslide distributions from 2007–2019 within a 30 km radius of each IMD hydrometric observatory in each of the sub-catchments. The NERI considered here is characterized by the Ganga (its tributary Mahananda) and Brahmaputra River basin systems (major tributaries include Teesta, Manas, and Subansiri) and their numerous tributaries (Figures S1). The climatic pattern of the region shows a distinct Southwest monsoon season from June to September and westerly disturbances from October to March(Sarkar et al., 2006; Saitluanga et al., 2021). The temperatures in the plains range from 15°C in January to 28°C in August, while hilly areas experience temperatures varying from 9°C in January to 21°C during monsoon seasons (Shrestha and Devkota, 2010). The annual rainfall often exceeds 1200 mm, supporting a rich diversity of forest cover from evergreen to semi-evergreen types (Singh et al., 2021).

We collected the daily meteorological records from eight hydrometric observatories for the period 1980 to 2019: Aizawl (in Mizoram), Darjeeling (in West Bengal), Gangtok (in Sikkim), Kalimpong (in West Bengal), Kohima (in Nagaland), Guwahati (in Assam), Shillong (in Meghalaya), and Imphal (in

https://doi.org/10.5194/nhess-2024-152
Preprint. Discussion started: 19 September 2024


Natural Hazards and Earth System Sciences Discussions

Manipur) (Figure 1). We obtained the station-based daily rainfall time series with a few data gaps from the India Meteorological Department's (IMD) Data Supply Portal (https://dsp.imdpune.gov.in/). We choose daily temporal resolutions instead of hourly time scales to develop operational MDL thresholds at a regional scale. This is because of the limited to no-record availability of hourly records in several sites across the NERI. Second, daily forecasts are generally more reliable than hourly forecasts, providing credibility in an operational setting (Leonarduzzi and Molnar, 2020). We reconstructed the daily time series from intermittent temporal gaps by infilling each station record using openly accessible gridded daily rainfall records from the IMD (Pai et al., 2014) available at a high spatial resolution (0.25°, i.e., ~ 27.5 km), focusing on approximately 10-12 grids around each station, within a 50 km radius. Further, we compiled the comprehensive landslide catalogue by integrating landslide information from the NASA's Cooperative Open Online Landslide Repository (COOLR) (Kirschbaum et al., 2015) and the Geological Survey of India (GSI)'s Bhukosh Catalogue (https://bhukosh.gsi.gov.in). The compiled catalogue encompasses over eleven thousand MDLs recorded between 2007 and 2019. Local landslide events, particularly those triggered by rainfall in the NEH, were detailed through the GSI's landslide inventory, which, despite often lacking precise time stamps (in the form of dates and hours), provides valuable information for understanding the spatial and temporal distribution (from year information) of landslides.

3 Methods

We focused exclusively on MDLs, reflecting the significant impact of monsoonal and extreme precipitation events over the NERI. Prior to 2006, the lack of comprehensive landslide documentation suggests the unavailability of reliable landslide assessment and mapping in this region. Our catalogued landslide point information (in Table 1), indicates that between 2006 and 2019, 490 landslides were reported within a 30 km radius of each station. Of these, approximately 67% occurred during the monsoon season, highlighting the critical influence of seasonal rains on landslide triggers in this geomorphologically sensitive region. Figure 2 shows the detailed workflow for the analysis.

https://doi.org/10.5194/nhess-2024-152
Preprint. Discussion started: 19 September 2024


Natural Hazards and Earth System Sciences Discussions

3.1 Treatment of Missing Daily Rainfall Time Series

Addressing gaps in gauge-based rainfall time series often involves the application of machine learning techniques to reconstruct incomplete precipitation records (Kim and Pachepsky, 2010; Schneider, 2001). In this study, we utilized the RegEM method to infill the missing gaps in time series across multiple locations (Li et al., 2005). RegEM, a widely adopted method in climate research, employs regularized ridge regression for parameter estimation and leverages extended cross-validation to ensure accuracy (Houdouin et al., 2023; Schneider, 2001). Unlike the conventional EM algorithm, RegEM initializes with estimates derived from the nearest observations rather than selecting missing values randomly. This iterative procedure involves an initial guess followed by the estimation step (E-step), which computes the missing values using the initial parameters. The optimization continues with the maximization step (M-step) to refine the estimates, iterating until convergence is achieved, thereby ensuring robust reconstruction of the missing data points, i.e., rainfall observations (Li et al., 2005). The effectiveness of this approach in infilling missing rainfall records is well-documented in the literature (Feng et al., 2013; Stahle et al., 2020; Þórðarson et al., 2021).

To enhance the accuracy of our reconstructions, we considered seasonal stratifications rather than treating the entire year as a single time series. To reconstruct gauge-based missing rainfall, we utilized high-resolution (0.25°×0.25°) gridded daily rainfall records from the IMD (see Section 2). For each station, we selected rain grids within a 50 km radius, encompassing approximately 10–12 neighbouring grids per rain gauge. The 50 km search radius is consistent with previous assessments in areas with complex topography, enhancing the performance of the RegEM algorithm (Bellido-Jiménez et al., 2021; Livneh and Rajagopalan et al., 2017).

To evaluate the performance of the reconstructed time series, we compared them against the available observed rainfall series. For each season, randomly we discarded 30% rainfall records from the daily series, and then the efficacy of the infilled time series is evaluated using the RegEM algorithm using the multiple criteria (Beck et al., 2017). For rainfall magnitude, we analysed the mean annual precipitation (ΔMAP), differences at the 90% exceedance probability ($\Delta q10$), and the timing differences of the center of mass (ΔCOM) for observed versus simulated rainfall events using circular statistics (Stewart et al., 2005). Then we evaluate the efficacy of the temporal signatures using Spearman's rank correlation to

https://doi.org/10.5194/nhess-2024-152
Preprint. Discussion started: 19 September 2024


Natural Hazards and Earth System Sciences Discussions

measure the coherence between the daily and weekly time series of observed and the infilled time series. In particular, we utilize nonparametric Spearman's rank correlations, which mitigate the influence of outliers to compare the observed versus infilled daily and the 5-day accumulated rainfall records. To compute an overall score, we normalized rainfall signatures using the standard deviation of the observed time series, thereby emphasizing smaller values. The comprehensive accuracy of the reconstructed rainfall time series was quantified by calculating an overall performance score (Beck et al., 2017), integrating all five indices, with the final score being the median of the rainfall and temporal signatures.

3.2 Seasonal Rainfall Thresholds and Landslide Trigger Analysis

Identifying seasonal rain thresholds to identify rain events is crucial for understanding the patterns that lead to MDLs. The IMD typically classifies a rainy day with a threshold of 2.5 mm/day, but this measure fails to consider regional and seasonal differences (Segoni et al., 2018). To address this limitation, we adopt a rain threshold to define a 'rainy day' equivalent to 10% of the seasonal mean rainfall (Ratan and Venugopal, 2013). To determine these seasonal rain thresholds, the year is divided into four seasons: winter (January-March), summer (April-June), monsoon (July-September), and fall (October-December). Then we determine each season's threshold across sites by determining the number of rainy days per season with rainfall magnitude > 1 mm/day. The total seasonal accumulation (T_{sa}) is then determined as the sum of daily rainfall magnitudes. The mean seasonal rainfall (μ_{th}) is derived from the ratio between T_{sa} to the total number of rainy days. The seasonal threshold (Th) is then determined as 10% of the mean seasonal rainfall: $Th=\mu_{th} * 0.01$. Following this method, thresholds are calculated across all four seasons for each station.

We use the seasonal thresholds to analyze triggering and antecedent rainfall events and identify 'rainy days'. Following (Kim et al., 2021), a triggering rain event is defined as the continuous rainfall due to tropical cyclones, monsoon fronts, or localized convective storms and is assumed to begin following at least 24 hours without rain events (Figure S2). Antecedent rainfall, the cumulative rainfall preceding a triggering event, is crucial for assessing the likelihood of a landslide. Initially, we employed Crozier's formulation (Crozier and Eyles, 1980) to quantify AMC over the periods of 3, 5, 7, 11, 15, 21, 25, 30, 35, 40, 45, 50, 55, and 60 days (Kim et al., 2021), using a decay constant, K = 0.9. The choice of K is based

https://doi.org/10.5194/nhess-2024-152
Preprint. Discussion started: 19 September 2024


Natural Hazards and Earth System Sciences
Discussions

on drainage capacity and hydrological properties (Capecchi and Focardi, 1988). This constant proved effective even for capturing rainfall impacts of 60 days or more before landslides, considering both shallow to deep-seated landslides (Capecchi and Focardi, 1988):

$$ARx_n = KR_1 + K^2R_2 + \cdots + K^nR_n \quad (1)$$

where ARx_n is the antecedent rainfall for triggering event x. This approach enables precise measurement of antecedent rainfall, essential for determining the E-D thresholds and improving landslide predictability.

3.3 Determining the Optimal Time Lag for Rain-Triggered Landslides

Understanding the impact of AMC on landslide genesis necessitates identifying the optimal lag time to establish the correlation between antecedent rainfall and landslides. The review of the literature has shown that the effects of antecedent rainfall on landslide triggers vary with geological and precipitation characteristics, necessitating site-specific research. Prior evaluations have considered time lags ranging from 3 to 180 days depending on shallow to deep-seated (Das et al., 2023; Guzzetti et al., 2007) (Aleotti, 2004; Dikshit et al., 2019; Lazzari et al., 2018). In this study, cumulative antecedent rainfall was calculated at lag periods from 3 to 60 days. We consider two different criteria to identify an optimal time lag for landslide genesis: (i) Examining the correlation between triggering and antecedent rainfall events. (ii) The second criterion is based on establishing a simple quantitative relationship of normalized triggering versus normalized antecedent rainfall magnitudes. We evaluate a non-parametric scale-free measure, Kendall's τ correlation, to determine dependence between triggering and antecedent rainfall events. Given pairs (X_i,Y_i) and (X_j, Y_j) random variables, Kendall's τ is determined as: $\tau = \frac{N_c - N_d}{N_c + N_d}$,where N_c and N_d represent the number of concordant and discordant pairs, respectively. A τ value of +1 indicates perfect concordance, –1 indicates perfect discordance whereas 0 indicates independence. The *p*-value associated with Kendall's τ assesses the likelihood of a significant correlation (p-value < 0.10) at the 10% significance level under the null hypothesis of no correlation.

The next quantitative metric involved comparing the normalized triggering versus antecedent rainfall at various lag times (3, 5, 7, 15, 21, 25, 30, 35, 40, 45, 50, 55, and 60 days) using the following formula:

https://doi.org/10.5194/nhess-2024-152
Preprint. Discussion started: 19 September 2024


Natural Hazards and Earth System Sciences Discussions

$$X_n = \left(\frac{X - min(X)}{max(X) - min(X)}\right) \quad (2)$$

where X_n is the normalized value, X is the original data, $min(X)$ is the minimum value of the time series and $max(X)$ is the maximum value of the series. A graphical comparison of normalized values of triggering versus antecedent precipitation events reveals a 1:1 diagonal line in the graph, distinguishing the scattering bias with the assumption of an equal contribution from triggering versus antecedent rainfall to landslides (Dahal and Hasegawa, 2008). However, for a large array of sites, a graphical assessment of sites remains analytically intractable. Therefore, we determine the proportion of landslide points above and below the 1:1 reference line, assuming a square box of unit edge lengths correspond to different lag times to assess the contributions of daily rainfall at slope failure versus the AMC preceding the failure. This analysis aids in determining whether landslides is governed primarily by triggering events or antecedent rainfall.

3.4 Estimation of ED Thresholds Using Non-Crossing Quantile Regression

To establish at-site and regional ED MDL thresholds, first we determine the optimal time lag, estimating the role of AMC in landslide trigger. ED thresholds quantify the duration of rainfall events necessary to trigger landslides, providing a quantitative basis for predicting landslides. This is essential for early warning systems and risk management, particularly in landslide-prone areas (Guzzetti et al., 2007; Sarkar et al., 2023).

In this study, ED thresholds were estimated using non-crossing quantile regression, which calculates the conditional quantiles of a response variable (Liu and Wu, 2009). Unlike ordinary least squares regression that estimates the mean of the response variable, the quantile regression focuses on specific quantiles, offering a detailed understanding of the role of predictors in influencing the response variable distribution (Villarini and Slater, 2018). The method involves minimizing an asymmetrically weighted sum of absolute errors to estimate the intercept and slope for different quantiles. Considering training data $(x_i, y_i), \ldots, (x_n, y_n)$, the objective is to estimate the pth conditional quantile function $f_p(x)$, $P(Y \leq f_\tau(\boldsymbol{X})|\boldsymbol{X} = \boldsymbol{x})$= pth. Koenker and Bassett (1978) introduced the check function, $p_\tau(r)$, to estimate this function by minimizing the following objective function:

https://doi.org/10.5194/nhess-2024-152
Preprint. Discussion started: 19 September 2024


Natural Hazards and Earth System Sciences
Discussions

$$\min_{f_\tau} \sum_{i=1}^{n} p_\tau\left(y_i - f_\tau(x_i)\right) \quad (3)$$

To avoid overfitting and enhance generalization, a regularization framework is applied:

$$\min_{f_\tau \in \mathrm{F}} \sum_{i=1}^{n} p_\tau\left(y_i - f_\tau(x_i)\right) + \lambda J(f_\tau) \quad (4)$$

where $\lambda \geq 0$ is the regularization parameter, and $J(f_\tau)$ represents the roughness penalty of the function. $f_\tau(.)$.

Standard quantile regression can result in non-monotonic and inaccurate quantile estimations due to crossing quantile curves. To address this issue, non-crossing quantile regression, which ensures monotonicity and accuracy, was proposed in the literature (Liu and Wu, 2009). The approach involves the inclusion of a linear programming optimization routine (Eq. 5), incorporating non-crossing constraints for any positive definite kernel function K (·, ·), which is expressed as (Liu and Wu, 2009):

$$\min_{\mathrm{b}, \alpha_1, \ldots, \alpha_n} \sum_{i=1}^{n} p_\tau\left(y_i - b - \sum_{j=1}^{n} \alpha_j K(x_i, x_j)\right) + \lambda\, \alpha^T K \alpha \quad (5)$$

where $\boldsymbol{\alpha}$ is a vector of length n, and K is an $n \times n$ matrix with elements $K\ (x_i, x_j)$, b is the regression coefficients (slope). The estimated quantile function is given by:

$$\widehat{f_\tau}(x) = \hat{b} + \sum_{i=1}^{n} \widehat{\alpha_{kl}}\, K(x, x_i) \quad (6)$$

The k[th] quantile fit is provided by:

$$\widehat{f_{\tau k}}(x) = \widehat{b_k} + \sum_{i=1}^{n} \widehat{\alpha_{kl}}\, K(x, x_i) \quad (7)$$

the non-crossing version is solved as:

$$\min_{\mathrm{b}_{k+1} \boldsymbol{\alpha}_{(k+1)}} \lambda \boldsymbol{\alpha}_{k+1}^T \boldsymbol{K} \boldsymbol{\alpha}_{(k+1)} + \sum_{i=1}^{n} p_{\tau k+1}\left(y_i - b_{(k+1)} - \sum_{j=1}^{n} \alpha_{j(k+1)} K\left(x_i, x_j\right)\right) \quad (8)$$

subjected to constraints

$$\hat{b}_k + \sum_{j=1}^{n} \widehat{\alpha_{kl}}\ K\left(x_i, x_j\right) + \delta_0 \leq \hat{b}_{k+1} + \sum_{j=1}^{n} \widehat{\alpha_{(k+1)J}}\ K\left(x_i, x_j\right) for\ i = 1,2 \ldots n, \quad (9)$$

Following the literature (Schwanghart, 2023), we employ a MATLAB-based tool 'ncquantreg.m' for determining non-crossing polynomial quantile regression at different quantile levels:

$$E = a + b(D) \quad (10)$$

https://doi.org/10.5194/nhess-2024-152
Preprint. Discussion started: 19 September 2024


Natural Hazards and Earth System Sciences Discussions

where a and b are regression coefficients, and D is the event duration in days. This linear relationship provides a straightforward estimation of *ED* thresholds.

3.5 Environmental Controls in ED Threshold Variability

The ED thresholds across the eight stations exhibit significant spatial variability, driven by key environmental controls(Singh et al., 2024; Sørensen et al., 2006; Yesuph and Dagnew, 2019; Zhao et al., 2023). To identify the relative contributions of each of the environmental controls in triggering landslides, we employ a relative entropy-based approach, Mutual Information (MI) criteria, that measures the distance between two probability distributions of underlying variables (Zhou et al., 2022). MI quantifies the dependency between two variables, with higher MI values indicating greater interdependence. MI between two variables a and b is defined as:

$$MI(a;b) = H(a) - H(a|b) \quad (11)$$

where $H(a)$ represents the entropy of a, and $H(a|b)$ is the conditional entropy of a given b (Latham and Roudi, 2009). For our analysis, we selected a suite of environment controls: vegetation, crops, built area, bare ground, rangeland, elevation, slope, TWI, and CND (Gupta et al., 2024) within a 30-km radius of each site.

Further, we compared the geological compositions across stations, encompassing sedimentary, metamorphic, and igneous rocks. Sedimentary rocks, characterized by high jointing and shearing, facilitate rapid water infiltration, resulting in quick soil saturation and reduced shear strength (Zhuang et al., 2024). Conversely, metamorphic and igneous rocks exhibit higher cohesion and structural integrity, requiring higher rainfall magnitude to induce landslides (Schmidt, 2023). This comparison highlights the crucial role of geological characteristics in mediating rain thresholds for landslide initiation (Lu et al., 2024; Xu et al., 2024).

4 Results

4.1 Performance and Variability of the RegEM Method

Figure S3 delineates the efficacy of the RegEM method in addressing data gaps within the rainfall time series from 1980 to 2019 across all sites. The heat map showcases the performance scores of the RegEM

https://doi.org/10.5194/nhess-2024-152
Preprint. Discussion started: 19 September 2024

method, spanning from 0.99, indicative of excellent time series reconstruction, to 0.45, denoting a modest outcome. Notably, Guwahati and Shillong exhibit scores consistently above 0.8, underscoring the method's superior performance in these regions. In contrast, Aizwal and Kohima, characterized by fewer observations with significant data gaps, display variable effectiveness, with scores occasionally falling into the moderate range (0.4-0.6). This figure highlights the differential efficacy of the RegEM approach in managing missing rainfall data, dependency on the initial volume and quality of available data for achieving optimal performance over the full temporal spectrum.

The rain threshold distribution (Figure S4) for detecting rain events across different seasons reveals distinct seasonal and spatial variations. During the Southwest Monsoon, from June to September, the region encounters peak rainfall, with June typically recording the highest amounts. The analysis reveals that the monsoon season (July to September), shows the most pronounced rainfall thresholds, with a median value of 12.9 mm/day. In comparison, the summer season (April to June) presents a median threshold of 3.3 mm/day, while the fall (October to December) and winter (January to March) seasons both register considerably lower median thresholds of 1.0 mm/day. This temporal variability in seasonal rain thresholds underscores the sharp contrast in rainfall intensity between the monsoon and non-monsoon periods within the NEH region.

4.2 Correlation of Antecedent Rainfall at Different Lags versus Triggering Rain Events Showing Antecedent Rainfall Controls on Landslides

Figure 3 illustrates the Kendall's τ correlation coefficients between triggering rainfall events and antecedent accumulated rainfall across various time lags at selected sites with significant correlations ($p < 0.05$). Finally, the optimal time lag is selected considering the trade-offs between the highest correlation value and the scattering bias of daily rainfall at slope failure versus the AMC preceding the failure (see Section 3.3 for details). Figure S5 explores the agreement between normalized cumulative antecedent rainfall and triggering rainfall events across various time lags for Gangtok. Both the 30-day and 35-day lags show a significant bias toward normalized triggering rainfall with only 13% rainfall contribution to trigger landslides, highlighting the substantial influence of long-term antecedent moisture in landslide trigger (Figure S5). Despite similar biases at both 30- and 35-day lags, the 35-day time lag is selected as

https://doi.org/10.5194/nhess-2024-152
Preprint. Discussion started: 19 September 2024


Natural Hazards and Earth System Sciences Discussions

the optimal period due to its slightly stronger correlation with triggering rainfall events, offering a more reliable prediction of landslide events.

Figure 4 quantifies the scattering bias between triggering rainfall events and antecedent accumulated rainfall across varying lag times up to 60 days. In Gangtok, this bias stabilizes beyond the 35-day lag, where landslide occurrences are predominantly driven by long-term antecedent moisture, with a pronounced bias toward lower triggering rainfall values. Imphal shows a preference for shorter-term antecedent rainfall, with the highest landslide activity occurring at a 25-day lag. Kalimpong also identifies a 25-day lag as optimal, reflecting a similar pattern. Darjeeling demonstrates a strong association at a 15-day lag. In contrast, Shillong, Kohima, Aizwal, and Guwahati show peaks at an 11-day lag, underscoring the consistent impact of short-term antecedent moisture across these locations. Table 2 summarizes these optimal lag times, identifying critical periods ranging from 11 to 35 days, and provides key insights into the interaction between triggering rainfall and antecedent conditions, a crucial step in calculating regional ED thresholds.

Following the above criteria, for Darjeeling, we selected a 15-day lag ($\tau \approx 0.84$), while for Kalimpong, a 25-day time lag ($\tau \approx 0.57$) emerged as optimal. Imphal, in contrast, shows positive correlations at 15-day and 21-day lags, with the 25-day lag ($\tau \approx 0.41$) selected as optimal considering the scattering bias between triggering and antecedent rainfall at d = 25-day time lag (Figure 3). The analysis also highlights instances where no significant correlations were observed, indicating that Kendall's τ correlation alone may not be adequate to assess the impact of AMC on MDL trigger.

4.3 ED Threshold Analysis

Figure 5 illustrates the ED thresholds for landslide prediction across multiple locations, using non-crossing quantile regression to analyze varying rainfall percentiles ranging from 10^{th}, $20^{th,}$ and 50^{th} percentiles. We determine the ED MDL thresholds for each site considering the ideal time lags for the AMC that vary from 11 to 35 days (Table 2) across different sites of the NEH. A few sites, *e.g.,* Aizwal, Imphal, and Kalimpong, require less rainfall to trigger landslides compared to Guwahati and Shillong.

https://doi.org/10.5194/nhess-2024-152
Preprint. Discussion started: 19 September 2024


Natural Hazards and Earth System Sciences Discussions

This differential response is quantified in Table S1**,** detailing the intercepts and slopes considering the 20th percentile rain thresholds. Apparently, the slope for the rain thresholds at Shillong is the highest, whereas Imphal offers the lowest slope for triggering rain-induced landslides.

Figure S6 displays the ROC-AUC curves for a few representative sites, namely, Gangtok, Kohima, and Kalimpong, validating the effectiveness of the derived ED thresholds for landslide prediction through non-crossing quantile regression. Gangtok, with an AUC of 0.78, demonstrates robust predictive capability, indicating the effectiveness of the developed model. Likewise, Kohima and Kalimpong show strong predictive performance with AUC values of 0.76 and 0.75, respectively. These results highlight the credibility of the derived thresholds.

Figure 6 portrays aggregated rainfall thresholds triggering MDLs considering all eight sites across the NEH, representing the regional ED thresholds (Eq. 14). The figure further compares these regional ED threshold curves, derived using non-crossing quantile regression, with two global thresholds: one representing both shallow and deep-seated landslides (Eq. 12) and the other specifically for deep-seated landslides (Eq. 13), proposed by Guzzetti et al (2007). All three equations are shown below:

$$E = 14.82\, D^{0.61} \qquad Range\ \ 0.167\ [hr] < D < 500 \tag{12}$$

$$E = 4.93\, D^{0.504} \qquad Range\ \ 0.1\ [hr] < D < 100 \tag{13}$$

$$E = -11.10 + 0.62\, D \qquad Range\ \ 24\ [hr] < D < 1440 \tag{14}$$

where E represents accumulated rainfall (mm) and D is rainfall duration (hours). The NEH regional threshold (Eq. 4.3) lies well within the global thresholds for deep and shallow landslides and aligns closely with the global threshold curves for the shallow landslide, represented by the black curve. The NEH threshold is lower than the global shallow threshold curves for short durations, whereas the discrepancy between both curves increases at longer durations. This could be possibly due to the sparser observation records. This figure highlights the importance of region-specific ED thresholds for landslide prediction and disaster management in the NEH region, underpinning the need to consider both trigging events and accumulated rain events for threshold derivation.

https://doi.org/10.5194/nhess-2024-152
Preprint. Discussion started: 19 September 2024


Natural Hazards and Earth System Sciences
Discussions

4.4 Geospatial Variability in Rainfall Thresholds

Figure 7 shows a comparative analysis of 3-day and 7-day accumulated rainfall thresholds across the NEH, with the rain threshold map (a) representing the 3-day accumulation and the map (b) illustrating the 7-day accumulation necessary to trigger landslides. The spatial distribution of rainfall thresholds reveals significant regional variability. Notably, Guwahati and Shillong exhibit the highest rainfall thresholds, with 3-day accumulations reaching up to 91.8 mm and 66.3 mm, respectively, and the 7-day accumulations showing the rain thresholds to trigger landslides are 239.5 mm and 163.9 mm, respectively. In contrast, Aizwal and Imphal show considerably lower thresholds, with 3-day accumulations of 29.3 mm and 27 mm, whereas 7-day accumulations of 61.7 mm and 64.1 mm, respectively. The spatial variations could be attributed to the diverse geological, vegetative, and elevational conditions across the sites. In particular, the dense forests and solid rock formations in Guwahati and Shillong are likely to necessitate substantially more rainfall to initiate landslides, consistent with an earlier assessment (Peruccacci et al., 2017).

Figure S7 comprehensively assesses the top three LULC classes for each site and the corresponding rainfall thresholds, aiming to capture and understand the variability in rainfall thresholds across different sites of the NEH. For instance, almost all sites predominantly feature vegetation, except for Imphal, where crop land a is major land use type. Likewise, Gangtok is characterized by bare ground, whereas Guwahati is characterized by water bodies (~18%). This spatial variability in major LULC features potentially controls the rain thresholds to trigger MDLs.

Figure 8 shows the contribution of different environmental drivers to control the rainfall thresholds to trigger MDLs based on MI analysis. Elevation, with a MI value of 0.53, is the most critical control dictating the rain threshold. This is followed by the vegetation with an MI of 0.52, indicating its robust control in rain threshold. Rangeland (MI = 0.49) and CND (MI = 0.48) also play a significant role, influencing the water movement and its distribution in the landscape and contributing to the landslide trigger (Deliveris et al., 2023). Other drivers, e.g., bare ground, slope, TWI, and built areas, though less influential, still mediate rain thresholds to trigger landslides with MI values ranging from 0.37-0.44.

https://doi.org/10.5194/nhess-2024-152
Preprint. Discussion started: 19 September 2024


Natural Hazards and Earth System Sciences
Discussions

5 Discussion

5.1 Multi-hazard Risk in the Himalayan Region

Landslides represent a significant hazard in the Himalayan region, particularly those driven by moisture, is a typical multi-hazard event that involves compound interactions of multiple hazard drivers within a limited time window, *e.g.*, heavy rainfall, flash floods, debris flows, and slope instability, leading to slope failures (Gill and Malamud, 2014). Extreme precipitation in NEH often triggers cascades of such natural hazards, compounding the risks and quantification of associated uncertainties and challenging disaster management (He et al., 2023; Sharma et al., 2024). Our study provides key insights into the predictability and effectiveness of LEWS within the NERI by establishing robust rainfall thresholds and examining the critical role of *d*-day lagged AMC in landslide initiation. Understanding and addressing the interplay of such hazards is vital for enhancing regional resilience and developing integrated disaster mitigation strategies across high mountain Asia (March et al., 2024).

5.2 Spatial Variability in Rainfall Thresholds

Our analysis reveals significant spatial variability in rainfall thresholds across the NEH region, influenced by environmental controls, *e.g.*, elevation, LULC, slope, TWI, CND, and geological conditions. Guwahati and Shillong show notably higher rainfall thresholds, requiring substantial rainfall accumulations over both short and extended periods to trigger landslides. In contrast, Aizwal and Imphal exhibit much lower rain thresholds to trigger slides, indicating the diverse geological and environmental controls that contribute to varying levels of landslide susceptibility. The geological characteristics at each station also potentially play a crucial role in this variability. For example, Aizawl, with sedimentary rocks, e.g., sandstone, siltstone, and shale, is more prone to landslides even with moderate rainfall due to rapid water infiltration and reduced shear strength (Lalmuankimi, 2021; Lee et al., 2024). Conversely, the presence of metamorphic rocks, such as gneiss and schist, in Darjeeling contributes to higher rain thresholds due to their resistance to erosion (Prakash and Tewari, 2015). Due to their complex geological formations, Kalimpong and Gangtok, characterized by weathered rocks, exhibit moderate to lower thresholds, respectively, influenced by their unique geological conditions (Bhasin et al., 2023; Roy et al., 2022; Sengupta and Nath, 2022). Likewise, Kohima and Imphal, primarily characterized by fractured and

https://doi.org/10.5194/nhess-2024-152
Preprint. Discussion started: 19 September 2024

permeable rock types, experience increased landslide risks due to high water saturation (Singh and Okendro, 2023; Nokendangba Chang et al., 2021; Xu et al., 2021). Guwahati and Shillong, with robust granitic and gneissic formations, generally require higher rainfall to trigger landslides, though localized weathering can reduce these thresholds (Doley et al., 2021). These details highlight the necessity for region-specific thresholds integrating geological and environmental controls into the development of predictive models, thereby enhancing the precision and effectiveness of early warning systems in the NEH region (Bhusan and Goswami, 2013; Sarma et al., 2020).

5.3 Limitations and Future Directions

Our study, focused on the NERI, provides valuable insights into establishing rainfall thresholds for landslide prediction. We utilized high-resolution, station-based reconstructed daily rainfall records to derive rain thresholds considering both triggering and antecedent rainfall. A few caveats are worth highlighting. The sparse historical rainfall availability and uncertainty in landslide inventories introduce additional sources of uncertainties, which are common issues in investigating MDL thresholds triggering slides. Additionally, our analysis did not consider the impact of snowmelt-driven moisture contribution, which significantly contributes to antecedent moisture and influences rain thresholds to trigger landslides in the Himalayan region (Caracciolo et al., 2017). Furthermore, rain-on-snow events (rainfall + snowmelt) can increase soil saturation, particularly in areas where glacial meltwater is identified as another common driver for triggering shallow slides (Rautela et al., 2023; Wang et al., 2021).

Future research can be directed towards integrating deep causal learning-based approaches to improve the predictability of rainfall thresholds (Tesch et al., 2023). By incorporating complex interactions between meteorological, geological, and environmental drivers, including snowmelt and atmospheric conditions, deep learning models could significantly improve early warning systems, providing timely and precise alerts, contributing to the advancement of landslide emergency planning and improving societal resilience. In addition, validating these novel approaches across broader geographic contexts and evaluating rainfall thresholds across landslide-prone areas across the globe will be essential for generalizing the results and ensuring resilience to such hazards, facilitating climate change adaptation efforts (Hussain et al., 2023; Nava et al., 2023; Luna et al., 2024).

https://doi.org/10.5194/nhess-2024-152
Preprint. Discussion started: 19 September 2024


Natural Hazards and Earth System Sciences Discussions

6. Conclusions

This study provides crucial insights into the landslide susceptibility of the NEH region, with several key findings:

- Our analysis identified significant variability in the optimal lag periods for antecedent rainfall, ranging from 11 to 35 days across the study sites. Notably, four stations—Guwahati, Shillong, Kohima, and Aizwal—exhibited an optimal lag period of 11 days, highlighting the importance of considering short-term antecedent moisture conditions in triggering landslides. In contrast, Gangtok identified a 35-day lag, reflecting the need for considering longer-term moisture accumulation in certain areas. This variability underscores the necessity of tailoring LEWS to account for local conditions.
- Guwahati and Shillong emerged as the regions with the highest rainfall thresholds, requiring 91.8 mm and 66.3 mm over 3 days, and 239.5 mm and 163.9 mm over 7 days, respectively, to initiate landslides. These thresholds are significantly higher compared to sites, *e.g.*, Aizwal and Imphal, where the rain threshold requirement to trigger slides is relatively lower. This spatial variation in rain thresholds highlights the distinct susceptibility of different locations to rainfall-induced landslides.
- Our analysis underscores the paramount importance of elevation in determining rainfall thresholds for landslide initiation across the NEH region. Higher elevations contribute to increased gravitational forces on saturated slopes, necessitating more substantial rainfall to trigger landslides (Chicas et al., 2024). Similarly, dense vegetation acts as a stabilizing force by enhancing soil cohesion and reducing surface runoff, which also raises the thresholds required for landslide initiation (Rengers et al., 2020). Rangeland and CND further shape how water is distributed across the landscape, influencing the moisture content variability and its role in landslide triggers (Deliveris et al., 2023). Our analysis highlights the interactions of environmental controls and basin geologic conditions in shaping rain thresholds to trigger landslides.

The insights from this study add value to developing region-specific rainfall thresholds that incorporate the significant influence of geological and hydrological controls in landslide prediction

https://doi.org/10.5194/nhess-2024-152
Preprint. Discussion started: 19 September 2024

and risk management. Our method, which combines advanced data reconstruction techniques with non-crossing quantile regression, provides a strong quantitative framework for developing credible LEWS for the NEH region. This approach not only enhances the accuracy of landslide predictions but also strengthens disaster preparedness and resilience in this vulnerable region.

***Competing Interests*:** The author declares no competing interests.

***Funding*:** This work did not receive any significant funding. The first author is supported by an MHRD scholarship from the Government of India for his doctoral studies at IIT Kharagpur, India. The authors are thankful to IIT Kharagpur for providing the necessary computational resources.

Code Availability: The code developed from this study is accessible via the following GitHub repository: https://github.com/danishmonga8/MoistureLandslideThresholds_NEHimalayas/tree/main. The RegEM code utilized as part this research is publicly available at https://climate-dynamics.org/software/ (last access: March 2023). The code for Non-crossing polynomial quantile regression used in this study is available at https://github.com/wschwanghart/ncquantreg (last access: February 2023).

Data Availability: Station-based daily rainfall time series data was retrieved from the India Meteorological Department (IMD)'s Data Supply Portal (https://dsp.imdpune.gov.in/) (last access: March 2023) . Gridded rainfall time series for the Northeastern Himalayan region was sourced from the archived records of IMD, accessible at https://www.imdpune.gov.in/Clim_Pred_LRF_New/Grided_Data_Download.html (last access: April 2023). The historical landslide inventory was obtained from the NASA Cooperative Open Online Landslide Repository (COOLR) and the Geological Survey of India's Bhukosh portal, available at https://catalog.data.gov/dataset/global-landslide-catalog-export and https://bhukosh.gsi.gov.in/Bhukosh/, respectively (last access: July 2023).

https://doi.org/10.5194/nhess-2024-152
Preprint. Discussion started: 19 September 2024

References

Abraham, M. T., Satyam, N., Pradhan, B., Segoni, S., and Alamri, A.: Developing a prototype landslide early warning system for Darjeeling Himalayas using SIGMA model and real-time field monitoring, Geosci. J., 26, 289–301, https://doi.org/10.1007/s12303-021-0026-2, 2022.

Aleotti, P.: A warning system for rainfall-induced shallow failures, Eng. Geol., 73, 247–265, https://doi.org/10.1016/j.enggeo.2004.01.007, 2004.

Beck, H. E., van Dijk, A. I. J. M., de Roo, A., Dutra, E., Fink, G., Orth, R., and Schellekens, J.: Global evaluation of runoff from 10 state-of-the-art hydrological models, Hydrol. Earth Syst. Sci., 21, 2881–2903, https://doi.org/10.5194/hess-21-2881-2017, 2017.

Bellido-Jiménez, J. A., Gualda, J. E., and García-Marín, A. P.: Assessing Machine Learning Models for Gap Filling Daily Rainfall Series in a Semiarid Region of Spain, Atmosphere, 12, 1158, https://doi.org/10.3390/atmos12091158, 2021.

Bhasin, R., Aslan, G., and Dehls, J.: Ground Investigations and Detection and Monitoring of Landslides Using SAR Interferometry in Gangtok, Sikkim Himalaya, GeoHazards, 4, 25–39, https://doi.org/10.3390/geohazards4010003, 2023.

Bhukosh: available at: https://bhukosh.gsi.gov.in/Bhukosh/MapViewer.aspx, last access: July 2023.

Bhusan, K. and Goswami, D. C.: Triggering Factors of Landslides and Determination of Rainfall Threshold: A Case Study from North East India, in: Landslide Science and Practice, Springer, Berlin, Heidelberg, 87–92, https://doi.org/10.1007/978-3-642-31337-0_11, 2013.

Bogaard, T. and Greco, R.: Invited perspectives: Hydrological perspectives on precipitation intensity-duration thresholds for landslide initiation: proposing hydro-meteorological thresholds, Nat. Hazards Earth Syst. Sci., 18, 31–39, https://doi.org/10.5194/nhess-18-31-2018, 2018.

Bourenane, H. and Bouhadad, Y.: Impact of Land use Changes on Landslides Occurrence in Urban Area: The Case of the Constantine City (NE Algeria), Geotech. Geol. Eng., 39, 1–21, https://doi.org/10.1007/s10706-021-01768-1, 2021.

Capecchi, F., and Focardi, P.: Rainfall and landslides: research into a critical precipitation coefficient in an area of Italy, Nat. Hazards, 3, 199–203, https://www.cabidigitallibrary.org/doi/full/10.5555/19901949460, 1988.

https://doi.org/10.5194/nhess-2024-152
Preprint. Discussion started: 19 September 2024

Caracciolo, D., Arnone, E., Conti, F. L., and Noto, L. V.: Exploiting historical rainfall and landslide data in a spatial database for the derivation of critical rainfall thresholds, Environ. Earth Sci., 76, 222, https://doi.org/10.1007/s12665-017-6545-5, 2017.

Chicas, S. D., Li, H., Mizoue, N., Ota, T., Du, Y., and Somogyvári, M.: Landslide susceptibility mapping core-base factors and models' performance variability: a systematic review, Nat. Hazards, https://doi.org/10.1007/s11069-024-06697-9, 2024.

Choo, K.-S., Choi, J.-R., Lee, B.-H., and Kim, B.-S.: Parameter Sensitivity Analysis of a Korean Debris Flow-Induced Rainfall Threshold Estimation Algorithm, Water, 16, 828, https://doi.org/10.3390/w16060828, 2024.

Crozier, M. J., and Eyles, R. J.: Assessing the probability of rapid mass movement, in: Proceedings of the 3rd Australia-New Zealand Conference on Geomechanics, Wellington, New Zealand, 2–47, 1980.

Dahal, R. K. and Hasegawa, S.: Representative rainfall thresholds for landslides in the Nepal Himalaya, Geomorphology, 100, 429–443, https://doi.org/10.1016/j.geomorph.2008.01.014, 2008.

Das, S. R. and Ganguli, P.: Predictability of rainfall induced-landslides: The case study of Western Himalayan Region, EGUsphere, 1–32, https://doi.org/10.5194/egusphere-2022-243, 2022.

Das, S., Sarkar, S., and Kanungo, D. P.: A critical review on landslide susceptibility zonation: recent trends, techniques, and practices in Indian Himalaya, Nat. Hazards, 115, 23–72, https://doi.org/10.1007/s11069-022-05554-x, 2023.

Deliveris, A. V., Theocharis, A. I., Zevgolis, I. E., and Koukouzas, N. C.: Finite Element Analysis of Rainfall Infiltration Effects on Open-Pit Coal Mines' Slope Stability, in: Selected Studies in Geotechnics, Geo-informatics and Remote Sensing, Cham, 179–181, https://doi.org/10.1007/978-3-031-43759-5_39, 2023.

Dikshit, A. and Satyam, D. N.: Estimation of rainfall thresholds for landslide occurrences in Kalimpong, India, Innov. Infrastruct. Solut., 3, 24, https://doi.org/10.1007/s41062-018-0132-9, 2018.

Dikshit, A., Sarkar, R., Pradhan, B., Acharya, S., and Dorji, K.: Estimating Rainfall Thresholds for Landslide Occurrence in the Bhutan Himalayas, Water, 11, 1616, https://doi.org/10.3390/w11081616, 2019.

https://doi.org/10.5194/nhess-2024-152
Preprint. Discussion started: 19 September 2024

Dixit, S., Siva Subramanian, S., Srivastava, P., Yunus, A. P., Martha, T. R., and Sen, S.: Numerical-model-derived intensity–duration thresholds for early warning of rainfall-induced debris flows in a Himalayan catchment, Nat. Hazards Earth Syst. Sci., 24, 465–480, https://doi.org/10.5194/nhess-24-465-2024, 2024.

Doley, D., Sarma, G., and Bhagabaty, B.: Nature of Biotites from the Granitoids of Guwahati and Mayong Areas of Shillong Plateau, Northeastern India and their Petrogenetic Significance, J. Geol. Soc. India, 97, 625–634, https://doi.org/10.1007/s12594-021-1737-8, 2021.

EM-DAT: International Emergency disaster database, available at: https://www.emdat.be, last access: April 2023.

Feng, S., Hu, Q., Wu, Q., and Mann, M. E.: A Gridded Reconstruction of Warm Season Precipitation for Asia Spanning the Past Half Millennium, https://doi.org/10.1175/JCLI-D-12-00099.1, 2013.

Froude, M. J. and Petley, D. N.: Global fatal landslide occurrence from 2004 to 2016, Nat. Hazards Earth Syst. Sci., 18, 2161–2181, https://doi.org/10.5194/nhess-18-2161-2018, 2018.

Gill, J. C. and Malamud, B. D.: Reviewing and visualizing the interactions of natural hazards, Rev. Geophys., 52, 680–722, https://doi.org/10.1002/2013RG000445, 2014.

Godt, J. W. and McKenna, J. P.: Numerical modeling of rainfall thresholds for shallow landsliding in the Seattle, Washington, area, in: Landslides and Engineering Geology of the Seattle, Washington, Area, vol. 20, edited by: Baum, R. L., Godt, J. W., and Highland, L. M., Geological Society of America, 0, https://doi.org/10.1130/2008.4020(07), 2008.

Gupta, V., Syed, B., Pathania, A., Raaj, S., Nanda, A., Awasthi, S., and Shukla, D. P.: Hydrometeorological analysis of July-2023 floods in Himachal Pradesh, India, Nat. Hazards, 120, 7549–7574, https://doi.org/10.1007/s11069-024-06520-5, 2024.

Guzzetti, F., Gariano, S. L., Peruccacci, S., Brunetti, M. T., Marchesini, I., Rossi, M., and Melillo, M.: Geographical landslide early warning systems, Earth-Sci. Rev., 200, 102973, https://doi.org/10.1016/j.earscirev.2019.102973, 2020.

Guzzetti, F., Peruccacci, S., Rossi, M., and Stark, C. P.: Rainfall thresholds for the initiation of landslides in central and southern Europe, Meteorol. Atmospheric Phys., 98, 239–267, https://doi.org/10.1007/s00703-007-0262-7, 2007.

https://doi.org/10.5194/nhess-2024-152
Preprint. Discussion started: 19 September 2024

Harilal, G. T., Madhu, D., Ramesh, M. V., and Pullarkatt, D.: Towards establishing rainfall thresholds for a real-time landslide early warning system in Sikkim, India, Landslides, 16, 2395–2408, https://doi.org/10.1007/s10346-019-01244-1, 2019.

He, J., Zhang, L., Xiao, T., Wang, H., and Luo, H.: Prompt Quantitative Risk Assessment for Rain-Induced Landslides, J. Geotech. Geoenvironmental Eng., 149, 04023023, https://doi.org/10.1061/JGGEFK.GTENG-10980, 2023.

Houdouin, P., Ollila, E., and Pascal, F.: Regularized EM Algorithm, in: Proceedings of the IEEE International Conference on Acoustics, Speech, and Signal Processing (ICASSP), 97–100, https://doi.org/10.1109/ICASSP49357.2023.10096439, 2023.

Hussain, M. A., Chen, Z., Zheng, Y., Zhou, Y., and Daud, H.: Deep Learning and Machine Learning Models for Landslide Susceptibility Mapping with Remote Sensing Data, Remote Sens., 15, 4703, https://doi.org/10.3390/rs15194703, 2023.

Intergovernmental Panel On Climate Change (Ipcc): Climate Change 2021 – The Physical Science Basis: Working Group I Contribution to the Sixth Assessment Report of the Intergovernmental Panel on Climate Change, 1st ed., Cambridge University Press, https://doi.org/10.1017/9781009157896, 2023.

Jain, N., Roy, P., Martha, T. R., Jalan, P., and Nanda, A.: Landslide Atlas of India (Mapping, monitoring and advance techniques using space-based inputs), NRSC special publication, NRSC/ISRO, Document No. NRSC-RSA-GSG-GMED-FEB2023-TR-0002167-V1.0, available at: https://www.isro.gov.in, last access: January 2023.

Jaiswal, P.: Landslide scenarios in North East Himalaya: Active and passive slope, Geological Survey of India, available at: https://msdma.gov.in, last access: July 2023.

Johnston, E. C., Davenport, F. V., Wang, L., Caers, J. K., Muthukrishnan, S., Burke, M., and Diffenbaugh, N. S.: Quantifying the Effect of Precipitation on Landslide Hazard in Urbanized and Non-Urbanized Areas, Geophys. Res. Lett., 48, e2021GL094038, https://doi.org/10.1029/2021GL094038, 2021.

Jordanova, G., Gariano, S. L., Melillo, M., Peruccacci, S., Brunetti, M. T., and Jemec Auflič, M.: Determination of Empirical Rainfall Thresholds for Shallow Landslides in Slovenia Using an Automatic Tool, Water, 12, 1449, https://doi.org/10.3390/w12051449, 2020.

Kim, J.-W. and Pachepsky, Y. A.: Reconstructing missing daily precipitation data using regression trees and artificial neural networks for SWAT streamflow simulation, J. Hydrol., 394, 305–314, https://doi.org/10.1016/j.jhydrol.2010.09.005, 2010.

Kim, S. W., Chun, K. W., Kim, M., Catani, F., Choi, B., and Seo, J. I.: Effect of antecedent rainfall conditions and their variations on shallow landslide-triggering rainfall thresholds in South Korea, Landslides, 18, 569–582, https://doi.org/10.1007/s10346-020-01505-4, 2021.

Kirschbaum, D., Stanley, T., and Zhou, Y.: Spatial and temporal analysis of a global landslide catalog, Geomorphology, 249, 4–15, https://doi.org/10.1016/j.geomorph.2015.03.016, 2015.

Koenker, R. and Bassett, G.: Regression Quantiles, Econometrica, 46, 33–50, https://doi.org/10.2307/1913643, 1978.

Lalmuankimi, C.: Petrological, Environmental Deposition and Tectonic-Provenance Study of Bhuban Sandstones in Neogene Succession of Aizawl district, Mizoram, J. Geol. Soc. India, 97, 907–914, https://doi.org/10.1007/s12594-021-1790-3, 2021.

Latham, P. E. and Roudi, Y.: Mutual information, Scholarpedia, 4, 1658, https://doi.org/10.4249/scholarpedia.1658, 2009.

Lazzari, M., Piccarreta, M., and Manfreda, S.: The role of antecedent soil moisture conditions on rainfall-triggered shallow landslides, Nat. Hazards Earth Syst. Sci. Discuss., https://doi.org/10.5194/nhess-2018-371, 2018.

Lee, J.-S., Pradhan, A. M. S., Song, C.-H., and Kim, Y.-T.: Lithological terrain-based rainfall thresholds for possible initiation of shallow landslides in South Korea, Stoch. Environ. Res. Risk Assess., 38, 175–191, https://doi.org/10.1007/s00477-023-02568-0, 2024.

Leonarduzzi, E. and Molnar, P.: Deriving rainfall thresholds for landsliding at the regional scale: daily and hourly resolutions, normalisation, and antecedent rainfall, Nat. Hazards Earth Syst. Sci., 20, 2905–2919, https://doi.org/10.5194/nhess-20-2905-2020, 2020.

Lepore, C., Arnone, E., Noto, L. V., Sivandran, G., and Bras, R. L.: Physically based modeling of rainfall-triggered landslides: a case study in the Luquillo forest, Puerto Rico, Hydrol. Earth Syst. Sci., 17, 3371–3387, https://doi.org/10.5194/hess-17-3371-2013, 2013.

Li, H., Zhang, K., and Jiang, T.: The regularized EM algorithm, in: Proceedings of the AAAI Conference on Artificial Intelligence, 807–812, available at: https://cdn.aaai.org/AAAI/2005/AAAI05-127.pdf, 2005.

Liu, W., Bai, R., Sun, X., Yang, F., Zhai, W., and Su, X.: Rainfall- and Irrigation-Induced Landslide Mechanisms in Loess Slopes: An Experimental Investigation in Lanzhou, China, Atmosphere, 15, 162, https://doi.org/10.3390/atmos15020162, 2024.

LIU, X., WANG, Y., and LEUNG, A. K.: Numerical investigation of rainfall intensity and duration control of rainfall-induced landslide at a specific slope using slope case histories and actual rainfall records, Bull. Eng. Geol. Environ., 82, 333, https://doi.org/10.1007/s10064-023-03359-1, 2023.

Liu, Y. and Wu, Y.: Stepwise multiple quantile regression estimation using non-crossing constraints, Stat. Interface, 2, 299–310, https://doi.org/10.4310/SII.2009.v2.n3.a4, 2009.

Livneh, B., and Rajagopalan, B.: Development of a gridded meteorological dataset over Java island, Indonesia 1985–2014, Sci. Data, 4, 170072, https://doi.org/10.1038/sdata.2017.72, 2017.

Lu, W., Xiao, Z., Chen, Y., Sun, J., and Chen, F.: Spatiotemporal Characteristics and Rainfall Thresholds of Geological Landslide Disasters in ASEAN Countries, Atmosphere, 15, 599, https://doi.org/10.3390/atmos15050599, 2024.

Luna, L., Carmona, M. I. A., Veh, G., Lewis, E., Ozturk, U., and Korup, O.: Urban landslides triggered under similar rainfall conditions in cities globally, EGU General Assembly 2024, Vienna, Austria, 26, 11010, https://doi.org/10.5194/egusphere-egu24-11010, 2024.

Mandal, P. and Sarkar, S.: Estimation of rainfall threshold for the early warning of shallow landslides along National Highway-10 in Darjeeling Himalayas, Nat. Hazards, 105, 2455–2480, https://doi.org/10.1007/s11069-020-04407-9, 2021.

March, A., Woolley, M., and Failler, P.: Integration of climate change mitigation and adaptation in Blue Economy planning in Africa, Mitig. Adapt. Strateg. Glob. Change, 29, 38, https://doi.org/10.1007/s11027-024-10133-5, 2024.

https://doi.org/10.5194/nhess-2024-152
Preprint. Discussion started: 19 September 2024

Mohon Singh, Kh. and Okendro, M.: Geological and Geotechnical Studies of Nungkao Landslide Along Imphal-Jiribam National Highway, NH-37, Manipur, India, in: Landslides: Detection, Prediction and Monitoring: Technological Developments, edited by: Thambidurai, P. and Singh, T. N., Springer International Publishing, Cham, 145–160, https://doi.org/10.1007/978-3-031-23859-8_7, 2023.

Monga, D. and Ganguli, P.: Moisture-Driven Landslides and Cascade Hazards in the Himalayan Region: A Synthesis on Predictive Assessment, in: Landslide: Susceptibility, Risk Assessment and Sustainability: Application of Geostatistical and Geospatial Modeling, edited by: Panda, G. K., Shaw, R., Pal, S. C., Chatterjee, U., and Saha, A., Springer Nature Switzerland, Cham, 267–294, https://doi.org/10.1007/978-3-031-56591-5_10, 2024.

NASA POWER: Prediction of Worldwide Energy Resources: Methodology - Precipitation, available at: https://power.larc.nasa.gov/docs/methodology/meteorology/precipitation, last access: March 2024.

Nava, L., Carraro, E., Reyes-Carmona, C., Puliero, S., Bhuyan, K., Rosi, A., Monserrat, O., Floris, M., Meena, S. R., Galve, J. P., and Catani, F.: Landslide displacement forecasting using deep learning and monitoring data across selected sites, Landslides, 20, 2111–2129, https://doi.org/10.1007/s10346-023-02104-9, 2023.

Nokendangba Chang, C., Ezung, M., Apon, M., Supongtemjen, Walling, T., and Thong, G. T.: Assessment of Landslides Along NH 29 in the Kevüza Area, Kohima, Nagaland, Indian Geotech. J., 51, 841–860, https://doi.org/10.1007/s40098-021-00566-z, 2021.

Pai, D., Sridhar, L., Rajeevan, M., Sreejith, O. P., Satbhai, N. S., and Mukhopadhyay, B.: Development of a new high spatial resolution (0.25° × 0.25°) long period (1901-2010) daily gridded rainfall data set over India and its comparison with existing data sets over the region, Mausam, 65, 1–18, https://doi.org/10.54302/mausam.v65i1.851, 2014.

Peruccacci, S., Brunetti, M. T., Gariano, S. L., Melillo, M., Rossi, M., and Guzzetti, F.: Rainfall thresholds for possible landslide occurrence in Italy, Geomorphology, 290, 39–57, https://doi.org/10.1016/j.geomorph.2017.03.031, 2017.

https://doi.org/10.5194/nhess-2024-152
Preprint. Discussion started: 19 September 2024

Poornima, R., Ramakrishnan, S., Priyatharshini, S., Poornachandhra, C., John, J. E., Ramya, A., and Dhevagi, P.: Climate Change Implications in the Himalayas, in: The Himalayas in the Anthropocene: Environment and Development, edited by: Borthakur, A. and Singh, P., Springer Nature Switzerland, Cham, 237–277, https://doi.org/10.1007/978-3-031-50101-2_11, 2024.

Prakash, D. and Tewari, S.: Garnet-sillimanite bearing gneisses from Darjeeling, eastern Himalaya: Textural relationship and P–T conditions, J. Earth Syst. Sci., 124, 1187–1199, https://doi.org/10.1007/s12040-015-0603-8, 2015.

Ramesh, M. V., Thirugnanam, H., Singh, B., Nitin Kumar, M., and Pullarkatt, D.: Landslide Early Warning Systems: Requirements and Solutions for Disaster Risk Reduction—India, in: Progress in Landslide Research and Technology, Volume 1 Issue 2, 2022, edited by: Alcántara-Ayala, I., Arbanas, Ž., Huntley, D., Konagai, K., Mikoš, M., Sassa, K., Sassa, S., Tang, H., and Tiwari, B., Springer International Publishing, Cham, 259–286, https://doi.org/10.1007/978-3-031-18471-0_21, 2023.

Ratan, R. and Venugopal, V.: Wet and dry spell characteristics of global tropical rainfall, Water Resour. Res., 49, 3830–3841, https://doi.org/10.1002/wrcr.20275, 2013.

Rautela, K. S., Kumar, D., Gandhi, B. G. R., Kumar, A., and Dubey, A. K.: Long-term hydrological simulation for the estimation of snowmelt contribution of Alaknanda River Basin, Uttarakhand using SWAT, AQUA - Water Infrastruct. Ecosyst. Soc., 72, 139–159, https://doi.org/10.2166/aqua.2023.176, 2023.

Ravindran, S. and Gratchev, I.: Prediction of Shallow Rainfall-Induced Landslides Using Shear Strength of Unsaturated Soil, Indian Geotech. J., 51, 661–672, https://doi.org/10.1007/s40098-020-00468-6, 2021.

Rengers, F. K., McGuire, L. A., Oakley, N. S., Kean, J. W., Staley, D. M., and Tang, H.: Landslides after wildfire: initiation, magnitude, and mobility, Landslides, 17, 2631–2641, https://doi.org/10.1007/s10346-020-01506-3, 2020.

Roy, P., Ghosal, K., and Paul, P. K.: Landslide susceptibility mapping of Kalimpong in Eastern Himalayan Region using a Rprop ANN approach, J. Earth Syst. Sci., 131, 130, https://doi.org/10.1007/s12040-022-01877-2, 2022.

https://doi.org/10.5194/nhess-2024-152
Preprint. Discussion started: 19 September 2024

Saha, S., and Bera, B.: Rainfall threshold for prediction of shallow landslides in the Garhwal Himalaya, India, Geosyst. Geoenviron., 3, 100285, https://doi.org/10.1016/j.geogeo.2024.100285, 2024.

Saitluanga, benjamin l, Lalchhandama, G., and Rinawma, P.: Climate Change and Variability in the Northeastern Himalayan Region of India, Landsc. Environ., 15, 53–64, https://doi.org/10.21120/LE/15/2/5, 2021.

Sarkar, S., Chandna, P., Pandit, K., and Dahiya, N.: An event-duration based rainfall threshold model for landslide prediction in Uttarkashi region, North-West Himalayas, India, Int. J. Earth Sci., 112, 1923–1939, https://doi.org/10.1007/s00531-023-02337-y, 2023.

Sarkar, S., Kanungo, D. P., Patra, A. K., and Kumar, P.: GIS Based Landslide Susceptibility Mapping – A Case Study in Indian Himalaya, in: Disaster Mitigation of Debris Flows, Slope Failures and Landslides, Proceedings of the Interpraevent International Symposium On Disaster Mitigation of Debris Flows, Slope Failures and landslides, Niigata, Japan, 25–29 September 2006, 617–624, 2006.

Sarma, C. P., Dey, A., and Krishna, A. M.: Investigation of Rainfall-Induced Landslides at the Hillslopes of Guwahati Region, Assam, in: Geotechnics for Natural Disaster Mitigation and Management, edited by: Krishna, A. M. and Katsumi, T., Springer, Singapore, 75–87, https://doi.org/10.1007/978-981-13-8828-6_7, 2020.

Schmidt, S. T.: Metamorphic Rocks: Some Basic Concepts, in: Transmitted Light Microscopy of Rock-Forming Minerals : An Introduction to Optical Mineralogy, edited by: Schmidt, S. T., Springer International Publishing, Cham, 161–178, https://doi.org/10.1007/978-3-031-19612-6_8, 2023.

Schneider, T.: Analysis of Incomplete Climate Data: Estimation of Mean Values and Covariance Matrices and Imputation of Missing Values, J. Clim., 14, 853–871, https://doi.org/10.1175/1520-0442(2001)014<0853>2.0.CO;2, 2001.

Schwanghart, W.: Non-crossing polynomial quantile regression, MATLAB Central File Exchange, available at: https://in.mathworks.com/matlabcentral/fileexchange/54953-non-crossing-polynomial-quantile-regression, last access: February 2023.

https://doi.org/10.5194/nhess-2024-152
Preprint. Discussion started: 19 September 2024

Segoni, S., Piciullo, L., and Gariano, S. L.: A review of the recent literature on rainfall thresholds for landslide occurrence, Landslides, 15, 1483–1501, https://doi.org/10.1007/s10346-018-0966-4, 2018.

Sengupta, A. and Nath, S. K.: Landslide Susceptibility Mapping in Gangtok, Sikkim Himalaya, in: Geospatial Technology for Environmental Hazards: Modeling and Management in Asian Countries, edited by: Shit, P. K., Pourghasemi, H. R., Bhunia, G. S., Das, P., and Narsimha, A., Springer International Publishing, Cham, 539–559, https://doi.org/10.1007/978-3-030-75197-5_24, 2022.

Setiya, P., Singh, M., and Nain, A. S.: Evaluating the performance of Grid IMD, NASA POWER, and MarkSim timeseries weather dataset for Uttarakhand Climatic Condition, Theor. Appl. Climatol., 155, 2657–2668, https://doi.org/10.1007/s00704-023-04787-5, 2024.

Sharma, N., Saharia, M., and Ramana, G. V.: High resolution landslide susceptibility mapping using ensemble machine learning and geospatial big data, CATENA, 235, 107653, https://doi.org/10.1016/j.catena.2023.107653, 2024.

Sharma, V. K.: Catastrophic Landslides in Indian Sector of Himalaya, in: Understanding and Reducing Landslide Disaster Risk: Volume 5 Catastrophic Landslides and Frontiers of Landslide Science, edited by: Vilímek, V., Wang, F., Strom, A., Sassa, K., Bobrowsky, P. T., and Takara, K., Springer International Publishing, Cham, 191–197, https://doi.org/10.1007/978-3-030-60319-9_22, 2021.

Shrestha, A. B., and Devkota, L. P.: Climate change in the Eastern Himalayas: observed trends and model projections, International Centre for Integrated Mountain Development (ICIMOD), Kathmandu, Nepal, 12 pp., https://doi.org/10.5555/20113241606, 2010.

Singh, B., Jeganathan, C., Rathore, V. S., Behera, M. D., Singh, C. P., Roy, P. S., and Atkinson, P. M.: Resilience of the Central Indian Forest Ecosystem to Rainfall Variability in the Context of a Changing Climate, Remote Sens., 13, 4474, https://doi.org/10.3390/rs13214474, 2021.

Singh, K. and Kumar, V.: Rainfall Thresholds Triggering Landslides: A Review, in: Sustainable Environment and Infrastructure, Cham, 455–464, https://doi.org/10.1007/978-3-030-51354-2_42, 2021.

Singh, V. P., Singh, R., Paul, P. K., Bisht, D. S., and Gaur, S.: Land Use Land Cover (LULC) Change Analysis, in: Hydrological Processes Modelling and Data Analysis: A Primer, edited by: Singh, V. P., Singh, R., Paul, P. K., Bisht, D. S., and Gaur, S., Springer Nature, Singapore, 127–145, https://doi.org/10.1007/978-981-97-1316-5_6, 2024.

Sørensen, R., Zinko, U., and Seibert, J.: On the calculation of the topographic wetness index: evaluation of different methods based on field observations, Hydrol. Earth Syst. Sci., 10, 101–112, https://doi.org/10.5194/hess-10-101-2006, 2006.

Stahle, D. W., Cook, E. R., Burnette, D. J., Torbenson, M. C. A., Howard, I. M., Griffin, D., Diaz, J. V., Cook, B. I., Williams, A. P., Watson, E., Sauchyn, D. J., Pederson, N., Woodhouse, C. A., Pederson, G. T., Meko, D., Coulthard, B., and Crawford, C. J.: Dynamics, Variability, and Change in Seasonal Precipitation Reconstructions for North America, https://doi.org/10.1175/JCLI-D-19-0270.1, 2020.

Stewart, I. T., Cayan, D. R., and Dettinger, M. D.: Changes toward earlier streamflow timing across western North America, J. Clim., 18, 1136–1155, https://doi.org/10.1175/JCLI3321.1, 2005.

Telegraph India: Mizoram faces severe landslides amid heavy monsoon rains, available at: https://epaper.telegraphindia.com/imageview/472423/23927735/73.html, last access: March 2024.

Tesch, T., Kollet, S., and Garcke, J.: Causal deep learning models for studying the Earth system, Geosci. Model Dev., 16, 2149–2166, https://doi.org/10.5194/gmd-16-2149-2023, 2023.

Þórðarson, A. F., Baum, A., García, M., Vicente-Serrano, S. M., and Stockmarr, A.: Gap-Filling of NDVI Satellite Data Using Tucker Decomposition: Exploiting Spatio-Temporal Patterns, Remote Sens., 13, 4007, https://doi.org/10.3390/rs13194007, 2021.

Tsunetaka, H.: Comparison of the return period for landslide-triggering rainfall events in Japan based on standardization of the rainfall period, Earth Surf. Process. Landf., 46, 2984–2998, https://doi.org/10.1002/esp.5228, 2021.

Villarini, G. and Slater, L. J.: Examination of Changes in Annual Maximum Gauge Height in the Continental United States Using Quantile Regression, J. Hydrol. Eng., 23, 06017010, https://doi.org/10.1061/(ASCE)HE.1943-5584.0001620, 2018.

Wang, X., Otto, M., and Scherer, D.: Atmospheric triggering conditions and climatic disposition of landslides in Kyrgyzstan and Tajikistan at the beginning of the 21st century, Nat. Hazards Earth Syst. Sci., 21, 2125–2144, https://doi.org/10.5194/nhess-21-2125-2021, 2021.

Whiteley, J. S., Chambers, J. E., Uhlemann, S., Wilkinson, P. B., and Kendall, J. M.: Geophysical Monitoring of Moisture-Induced Landslides: A Review, Rev. Geophys., 57, 106–145, https://doi.org/10.1029/2018RG000603, 2019.

Xu, Y., Schulz, W. H., Lu, Z., Kim, J., and Baxstrom, K.: Geologic controls of slow-moving landslides near the US West Coast, Landslides, 18, 3353–3365, https://doi.org/10.1007/s10346-021-01732-3, 2021.

Xu, Z., Xiao, Z., Zhao, X., Ma, Z., Zhang, Q., Zeng, P., and Zhang, X.: Derivation of Landslide Rainfall Thresholds by Geostatistical Methods in Southwest China, Sustainability, 16, 4044, https://doi.org/10.3390/su16104044, 2024.

Yesuph, A. Y. and Dagnew, A. B.: Land use/cover spatiotemporal dynamics, driving forces and implications at the Beshillo catchment of the Blue Nile Basin, North Eastern Highlands of Ethiopia, Environ. Syst. Res., 8, 21, https://doi.org/10.1186/s40068-019-0148-y, 2019.

Zhang, M. and Liu, J.: Controlling factors of loess landslides in western China, Environ. Earth Sci., 59, 1671–1680, https://doi.org/10.1007/s12665-009-0149-7, 2010.

Zhao, Y., Meng, X., Qi, T., Chen, G., Li, Y., Yue, D., and Qing, F.: Estimating the daily rainfall thresholds of regional debris flows in the Bailong River Basin, China, Bull. Eng. Geol. Environ., 82, 46, https://doi.org/10.1007/s10064-023-03068-9, 2023.

Zhou, H., Wang, X., and Zhu, R.: Feature selection based on mutual information with correlation coefficient, Appl. Intell., 52, 5457–5474, https://doi.org/10.1007/s10489-021-02524-x, 2022.

Zhuang, Y., Hu, X., He, W., Shen, D., and Zhu, Y.: Stability Analysis of a Rocky Slope with a Weak Interbedded Layer under Rainfall Infiltration Conditions, Water, 16, 604, https://doi.org/10.3390/w16040604, 2024.

https://doi.org/10.5194/nhess-2024-152
Preprint. Discussion started: 19 September 2024


Natural Hazards and Earth System Sciences Discussions

Table 1: Summary of rainfall-induced landslide incidents (2006-2019) within a 30 km radius of key hydrometric stations in the NEH region.

870

Station	**WMO ID**	**Latitude** (in degrees)	**Longitude** (in degrees)	**No. of Landslides** (30 km)
Aizwal	42727	23.73	92.73	19
Darjeeling	42295	27.05	88.27	47
Gangtok	42299	27.33	88.62	114
Kalimpong	42296	27.07	88.62	84
Kohima	42527	25.63	94.17	19
Guwahati	42410	26.1	91.58	53
Shillong	42516	25.57	91.87	47
Imphal	42623	24.77	93.9	11

https://doi.org/10.5194/nhess-2024-152
Preprint. Discussion started: 19 September 2024

Natural Hazards and Earth System Sciences
Discussions

Table 2: Summary of optimal time lags for landslide trigger across eight sites, highlighting critical lag durations and corresponding bias assessments.

Station Name	Optimal Lag Duration (days)	Kendall's τ (Optimal)	p-value (Optimal)	Bias (%)
Darjeeling	15	0.84	< 0.05	60.1
Kalimpong	25	0.57	< 0.05	58.8
Gangtok	35	0.31	< 0.05	86.7
Guwahati	11	0.76	0.53	69.2
Shillong	11	0.6	0.48	70
Kohima	11	0.4	< 0.05	73.3
Imphal	25	0.41	0.1	36.4
Aizwal	11	0.5	0.48	70

https://doi.org/10.5194/nhess-2024-152
Preprint. Discussion started: 19 September 2024

Natural Hazards and Earth System Sciences
Discussions

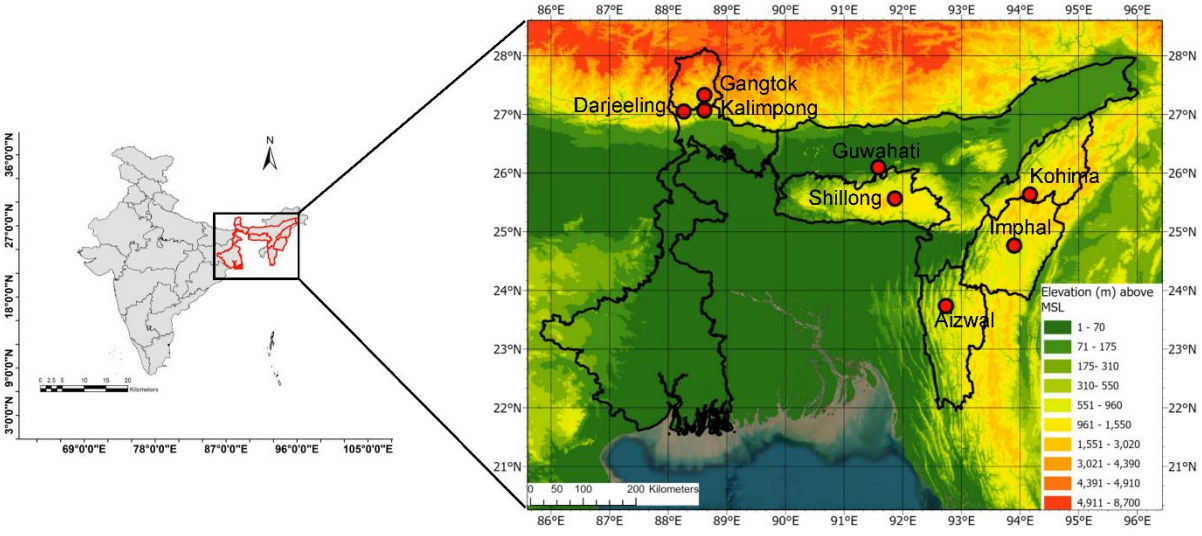

Figure 1: Schematics of NERI region showing the elevation map. The locations of eight hydrometric observatories under considerations are marked in red circles over the map. The inset on left shows the NERI (in red boundary) over India map.

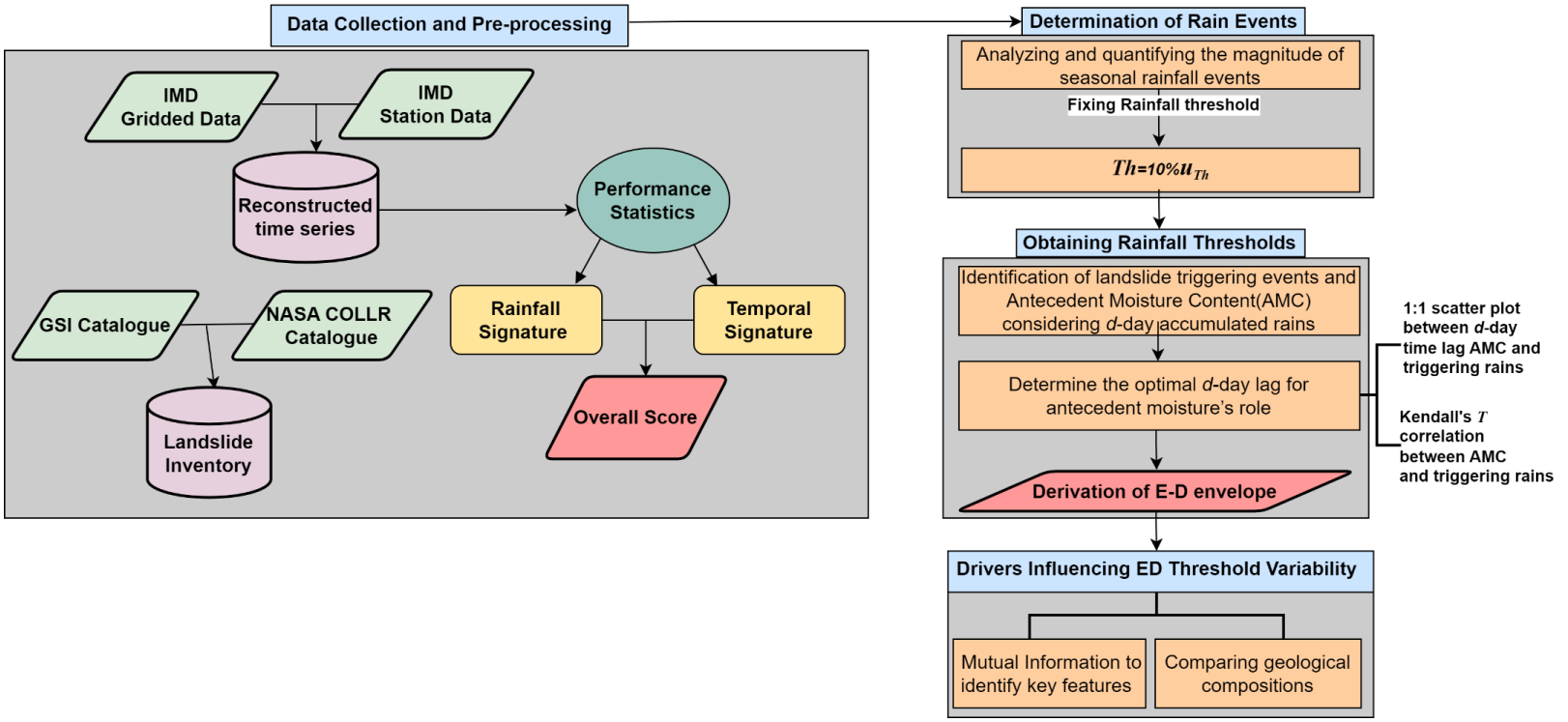

Figure 2: Detailed workflow of data collection, preprocessing, and analysis for establishing rainfall thresholds and understanding landslide dynamics in the NERI. The symbols Th and μ_{th}, representing seasonal thresholds and mean seasonal rainfall, respectively, are used throughout the flowchart to denote key analytical components of the study.

https://doi.org/10.5194/nhess-2024-152
Preprint. Discussion started: 19 September 2024

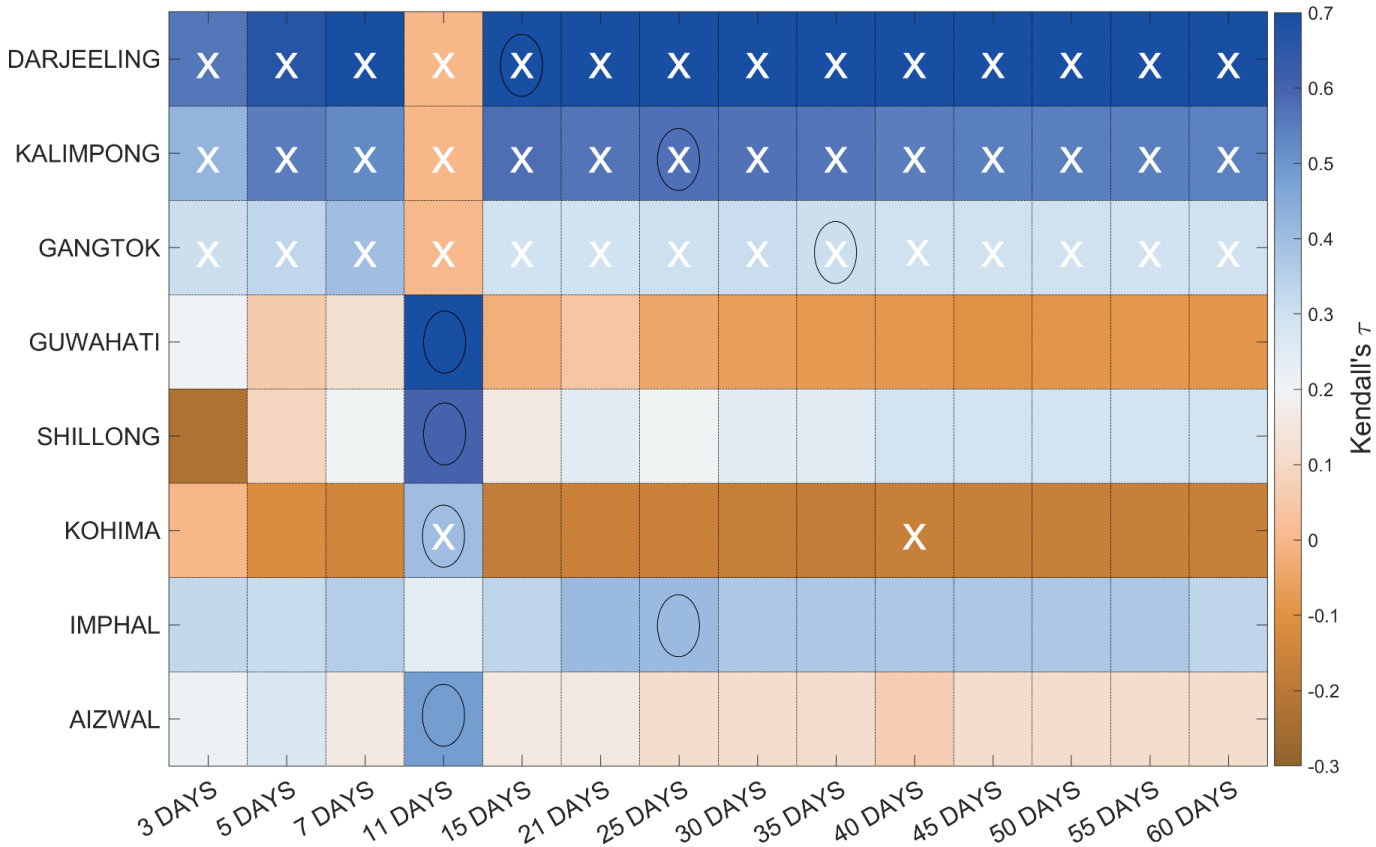

Figure 3: Kendall's τ correlation coefficients showing the correlation between antecedent rainfall accumulated over *d-day* time lag and the triggering rain events across representative gauges. Significant correlations ($p < 0.05$) are marked with 'X'. The ovals surrounding the 'x' symbols shows the optimal lag-time considering the trade-offs between significant correlation and scattering bias of triggering vs antecedent rainfall.

Natural Hazards and Earth System Sciences
Discussions
Open Access
EGU

https://doi.org/10.5194/nhess-2024-152
Preprint. Discussion started: 19 September 2024

Natural Hazards and Earth System Sciences
Discussions

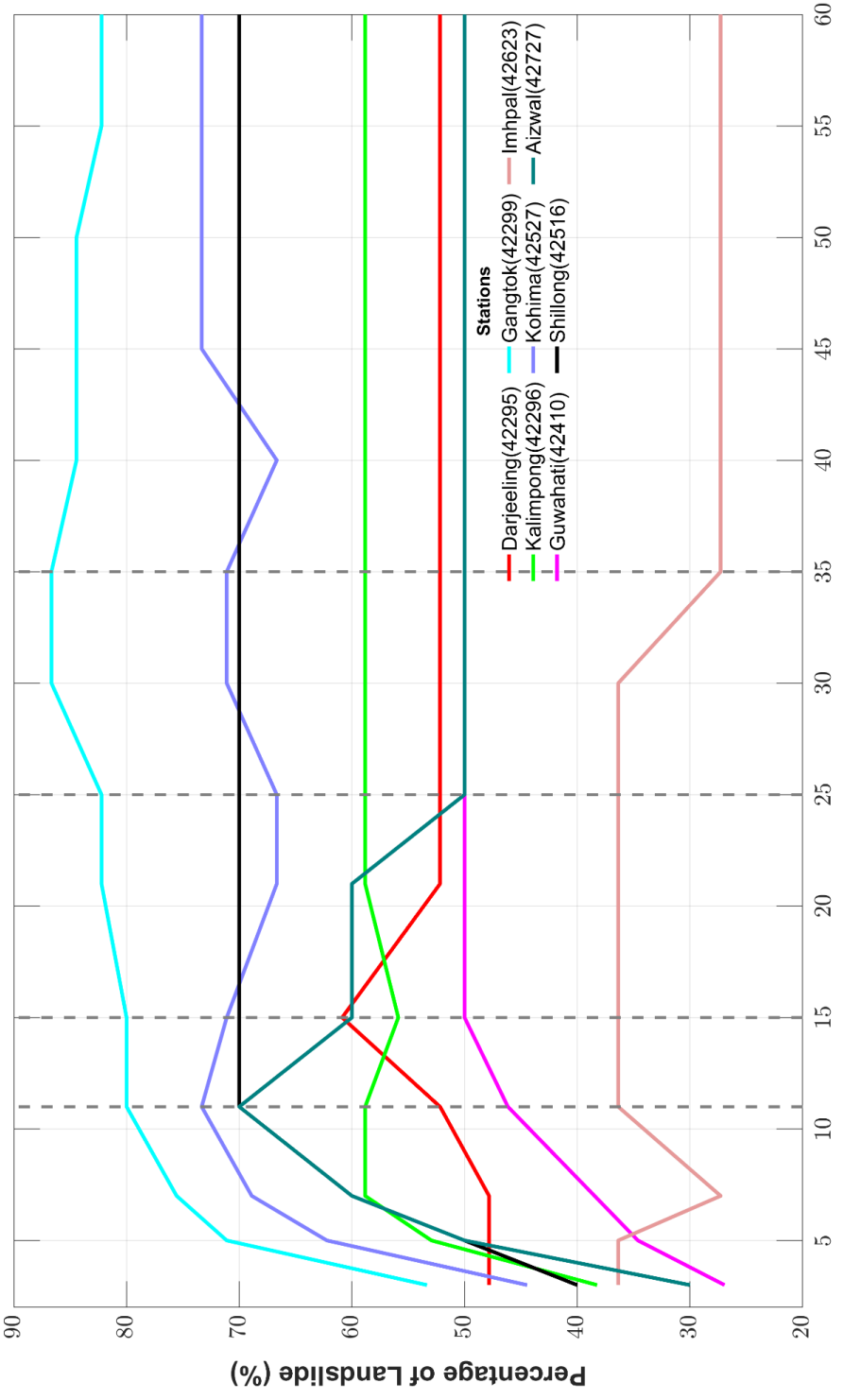

Figure 4 Landslide occurrences (in %) versus antecedent rainfall at different time lags. Dashed lines indicate the lag times corresponds to the highest frequency of landslides for each station.

https://doi.org/10.5194/nhess-2024-152
Preprint. Discussion started: 19 September 2024

Natural Hazards and Earth System Sciences
Discussions

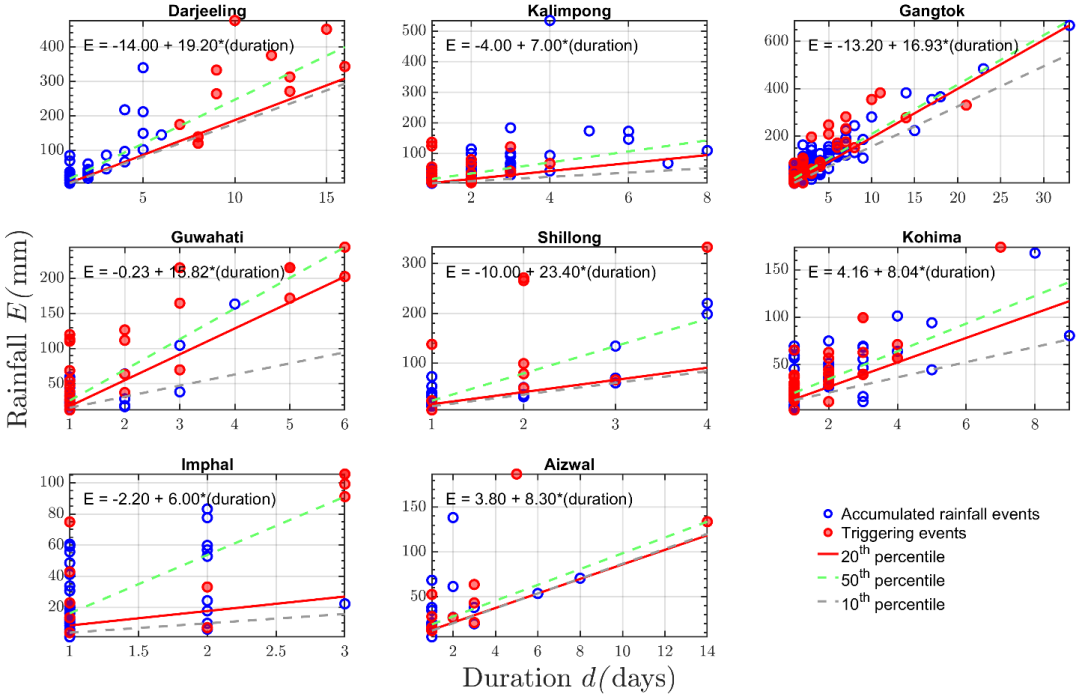

Figure 5: Empirical rain thresholds for cumulative rainfall Event (*E*) vs. Duration (*D*) at 10th (in grey), 20th (in red), and 50th (in green) percentiles, highlighting regional variations in landslide susceptibility with Guwahati and Shillong showing relatively higher thresholds, indicating low susceptibility.

https://doi.org/10.5194/nhess-2024-152
Preprint. Discussion started: 19 September 2024

Natural Hazards and Earth System Sciences
Discussions

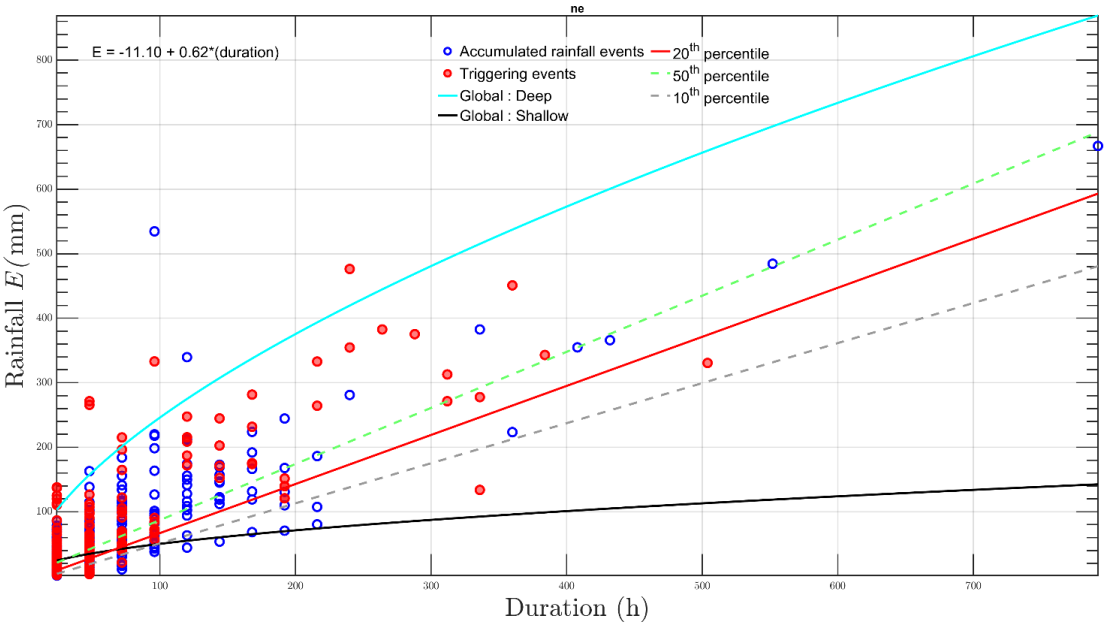

Figure 6: Empirical ED thresholds for the NERI at the 10th (in grey), 20th (in red), and 50th (in green) percentiles compared with global thresholds for deep (in cyan) and shallow (in black) landslides, indicating the regional susceptibility for shallow to deep landslides.

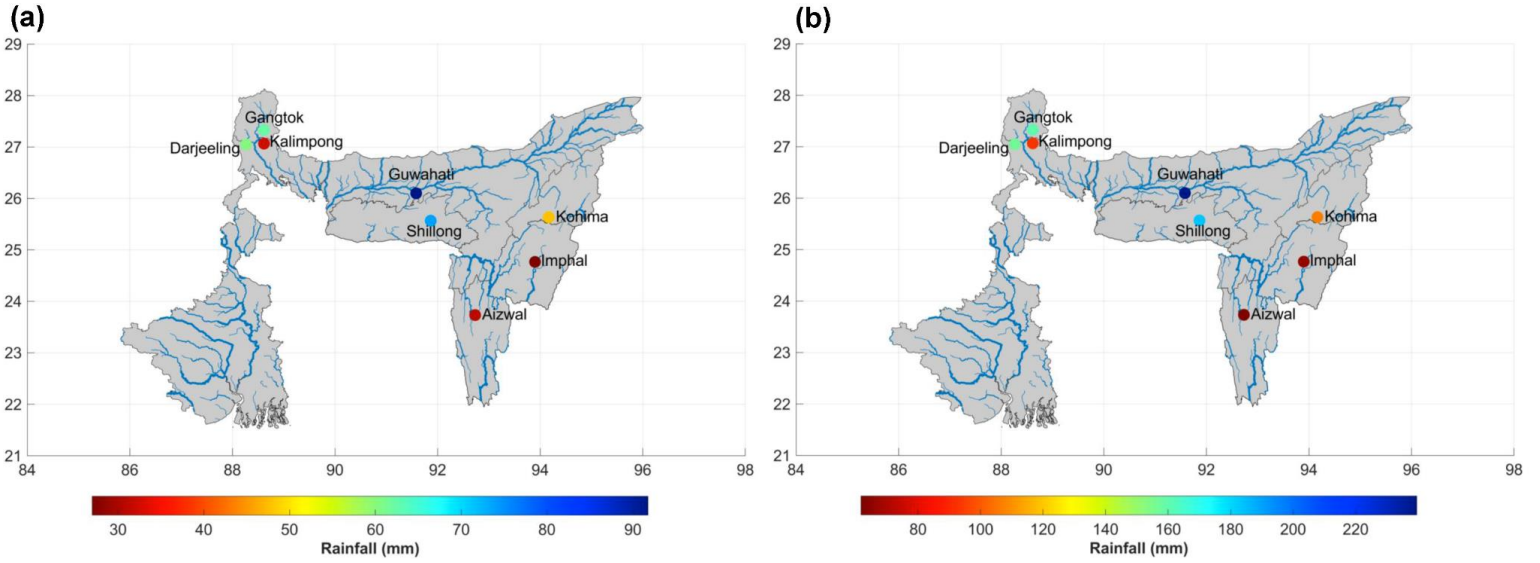

Figure 7: Spatial distribution of rain thresholds corresponding to event durations. (a) 3-day and (b) 7-day accumulated rainfall thresholds for landslide trigger in the NEH region. Guwahati and Shillong show the highest thresholds, indicating their greater resilience to triggering events.

https://doi.org/10.5194/nhess-2024-152
Preprint. Discussion started: 19 September 2024

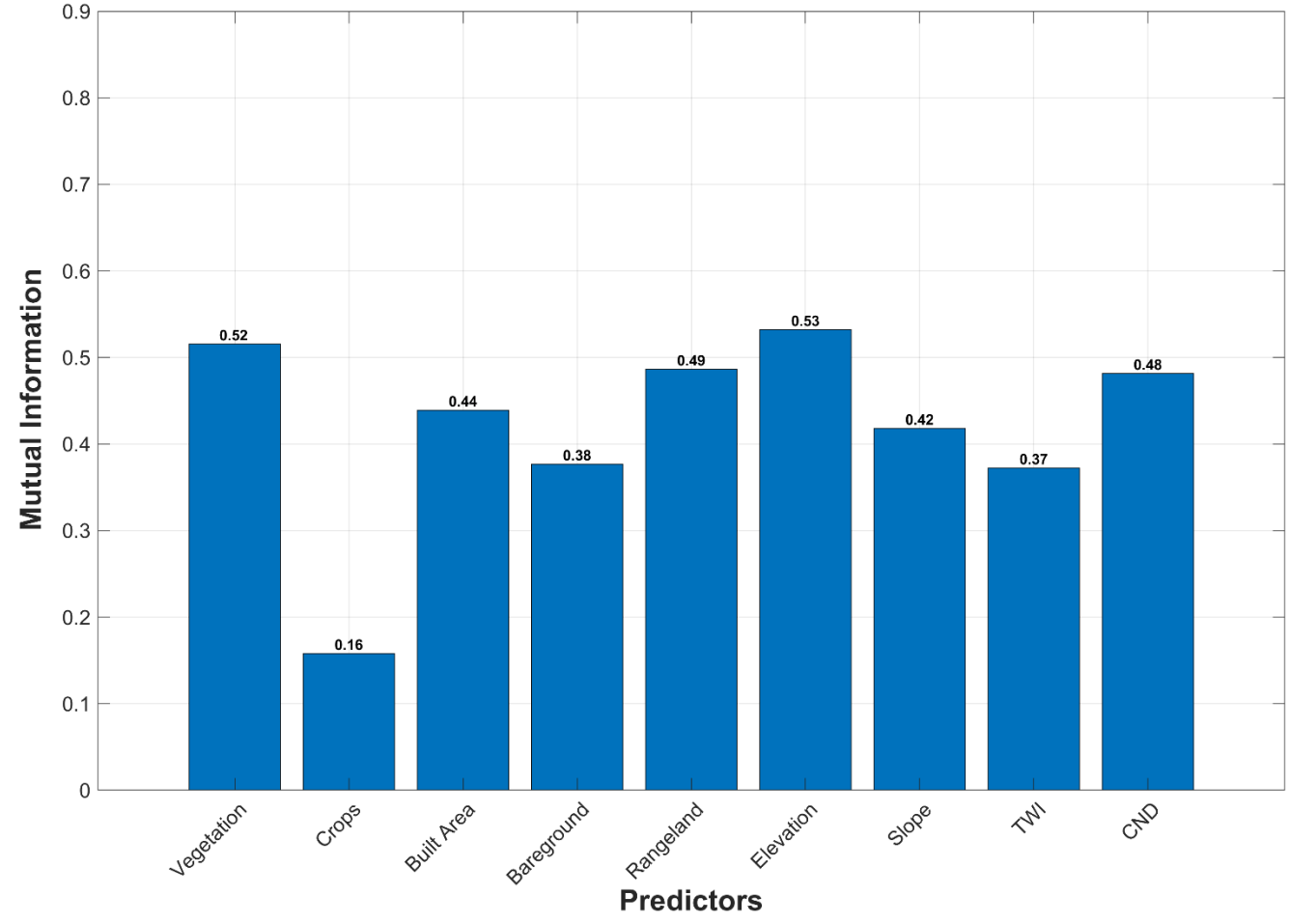

Figure 8: Mutual information (MI) of rainfall thresholds versus environmental controls for landslides across eight NERI stations